Accepted Manuscript

Fault and fracture patterns around a strike-slip influenced salt wall

G.I. Alsop, R. Weinberger, S. Marco, T. Levi

PII: S0191-8141(17)30238-9

DOI: 10.1016/j.jsg.2017.10.010

Reference: SG 3545

To appear in: *Journal of Structural Geology*

Received Date: 19 July 2017

Revised Date: 18 October 2017

Accepted Date: 29 October 2017

Please cite this article as: Alsop, G.I., Weinberger, R., Marco, S., Levi, T., Fault and fracture patterns around a strike-slip influenced salt wall, *Journal of Structural Geology* (2017), doi: 10.1016/j.jsg.2017.10.010.

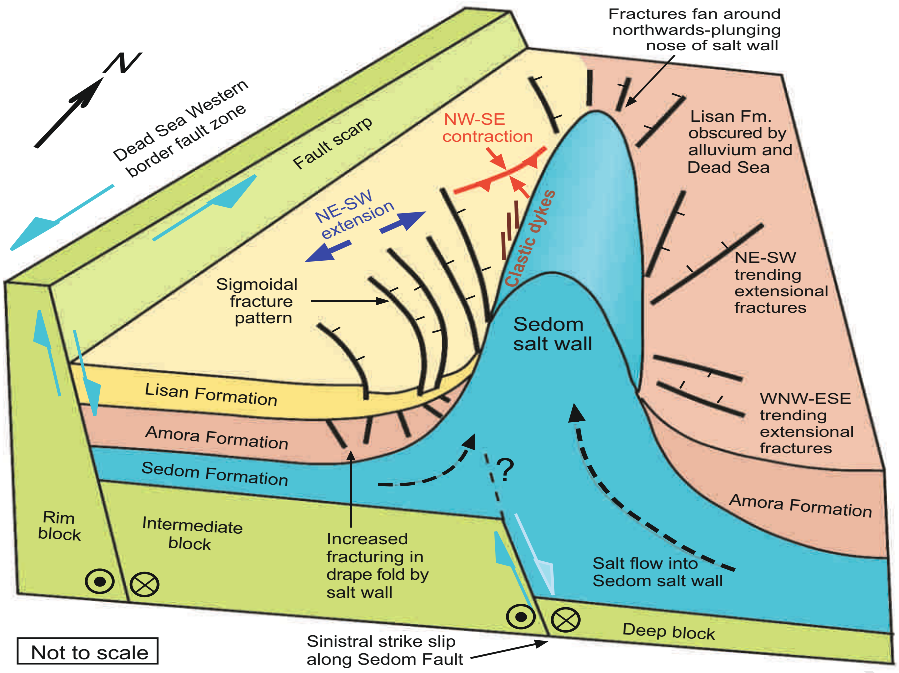

Fracture patterns are developed in overburden around an exposed salt wall in the Dead Sea Basin

Fracture patterns are neither concentric nor radial where diapirism is influenced by regional tectonics

Regional strike-slip faulting results in sigmoidal fracture traces developed at 45° to the salt wall

Extensional fractures accommodate upturn of bedding in drape folds

Fractures display a range of age relationships with the majority forming during drape folding

Fault and fracture patterns around a strike-slip influenced salt wall

G.I. Alsop[1], R. Weinberger[2, 3], S. Marco[4], T. Levi[2],
1) Department of Geology and Petroleum Geology, School of Geosciences,
University of Aberdeen, Aberdeen, UK. (e-mail: Ian.Alsop@abdn.ac.uk)
2) Geological survey of Israel, Jerusalem, Israel.
3) Department of Geological and Environmental Sciences, Ben Gurion University of the Negev, Beer Sheva, Israel.
4) Department of Geophysics, School of Geosciences, Tel Aviv University, Israel.

Abstract
The trends of faults and fractures in overburden next to a salt diapir are generally considered to be either parallel to the salt margin to form concentric patterns, or at right angles to the salt contact to create an overall radial distribution around the diapir. However, these simple diapir-related patterns may become more complex if regional tectonics influences the siting and growth of a diapir. Using the Sedom salt wall in the Dead Sea Fault system as our case study, we examine the influence of regional strike-slip faulting on fracture patterns around a salt diapir. This type of influence is important in general as the distribution and orientation of fractures on all scales may influence permeability and hence control fluid and hydrocarbon flow. Fractures adjacent to the N-S trending salt wall contain fibrous gypsum veins and injected clastic dykes, attesting to high fluid pressures adjacent to the diapir. Next to the western flank of the salt wall, broad (~1000 m) zones of upturn or 'drape folds' are associated with NW-SE striking conjugate extensional fractures within the overburden. Within 300 m of the salt contact, fracture patterns in map view display a progressive ~30°-35° clockwise rotation with more NNW-SSE strikes immediately adjacent to the salt wall. While some extensional faults display growth geometries, indicating that they were syn-depositional and initiated prior to tilting of beds associated with drape folding, other fractures display increasing dips towards the salt, suggesting that they have formed during upturn of bedding near the diapir. These observations collectively suggest that many fractures developed to accommodate rotation of beds during drape folding. Extensional fractures in the overburden define a mean strike that is ~45° anticlockwise (counter-clockwise) of the N-S trending salt wall, and are therefore consistent with sinistral transtension along the N-S trending Sedom Fault that underlies the salt wall. Our outcrop analysis reveals fracture geometries that are related to both tilting of beds during drape folding, and regional strike-slip tectonics. The presence of faults and fractures that interact with drape folds suggests that deformation in overburden next to salt cannot be simply pigeon-holed into 'end-member' scenarios of purely brittle faulting or viscous flow.
Keywords: Salt diapir, faults, fractures, Sedom, Dead Sea Fault system

1. Introduction
The trends of faults and fractures in overburden adjacent to a salt diapir are generally considered to be either parallel to the salt margin to form concentric patterns, or at right angles to the salt contact to create an overall radial distribution around the diapir (e.g. Jenyon, 1986, p.75; O'Brien and Lerch, 1987; Davison et al., 1996a, 2000a, b; Marco et al., 2002; Stewart, 2006; Yin and Groshong, 2007; Carruthers et al., 2013; Harding and Huuse, 2015; Dewing et al., 2016; Warren 2016, p. 536; Jackson and Hudec, 2017, p.104). Indeed, when summarising previous studies of fault patterns around circular salt diapirs or stocks, Wu et al. (2016, p.784) noted that "nearly all report radial and concentric faults in the roof and adjacent strata of salt diapirs". The concentric fault patterns reflect salt-induced pressure normal to the diapir walls (typically the maximum principal stress, σ1), while radial faults are created by circumferential 'hoop' stresses parallel to the salt margin (typically the

minimum principal stress, σ3) (e.g. Nikolinakou et al., 2014; Heidari et al., 2017 and references therein). However, it is also recognised that these simple diapir-related patterns may become more complex if regional tectonics influences the siting and growth of a diapir (e.g. Quinta et al., 2012 p.529; King et al., 2012; Wu et al., 2016). In this case, 'mixed patterns' of faults and fractures may occur that change geometry from being controlled by the regional stress field to being controlled by the sum of the regional and diapiric stresses approaching the salt (e.g. Quinta et al., 2012).

Salt walls may simply be defined as linear diapirs where the cross-sectional ratio is >2 (Hudec and Jackson, 2011, p.31). Although a number of recent studies have examined fracture patterns within overburden adjacent to buried or removed salt walls (e.g. Koestler and Ehrmann, 1987; Storti et al., 2011), they seldom consider the influence of regional tectonics on fracturing. In addition, the role that salt plays in regional strike-slip fault systems has been relatively poorly studied in comparison to extensional tectonic settings (e.g. see Jenyon, 1986, p.66), although it is widely recognised that salt diapirs form in extensional step-overs within the overall strike-slip fault zones (e.g. Koyi et al., 2008; Hudec and Jackson, 2011, p.81, Dooley and Schreurs, 2012; Fossen, 2016, p.435; Warren, 2016, p.766; Jackson and Hudec, 2017, p.336).

Owing to the solubility of halite, very few places exist where the detailed field study of fracturing and timing relationships around exposed salt diapirs can actually be undertaken. The influence of regional tectonics on fracturing will depend on its timing relative to salt emplacement, when for example, late-stage tectonics results in faults and fractures that simply cross-cut and overprint diapir-related deformation of overburden (e.g. Schorn and Neubauer, 2014). Those areas where halite is exposed are typically associated with orogenic contraction, resulting in salt being laterally squeezed to create surficial flows or salt glaciers, which may then mask fault patterns in adjacent overburden (e.g. Talbot, 1979; 1998; Aftabi et al., 2010; Colon et al., 2016). Many recent studies are potentially complicated by salt diapirs being overprinted by late-stage regional contraction. They include examples of salt diapirs from La Popa in Mexico (Giles and Rowan, 2012), NW China (e.g. Li et al., 2014), Sivas Basin in Turkey (e.g. Ringenbach et al., 2013; Callot et al., 2014; Kergaravat et al., 2017), Central High Atlas of Morocco (e.g. Martín-Martín et al., 2017) and northern Spain (e.g. Poprawski et al., 2014, 2016). This overprinting makes the interpretation of faults and fractures adjacent to salt more problematic due to the potential for reactivation of existing diapir-related faults and/or creation of new 'regional' faults. Establishing the timing of diapir emplacement relative to any regional deformation is therefore critical when interpreting patterns of faulting and fracturing around diapirs.

Although analysis of seismic sections may permit imaging of larger scale faulting around salt diapirs, the distribution and timing of many fractures can be difficult to ascertain due to steeply dipping beds around the flanks of the diapir, together with potential fluid movements adjacent to the salt (e.g. Davison et al., 2000a, b; Vandeginste et al., 2017; Luo et al., 2017). While drill cores and well logs may provide some help in estimating fracture intensity within the overburden (e.g. Davison et al., 2000a, b), they potentially suffer from limited and biased sampling depending on the orientation of the well, combined with possible reorientation and disaggregation during recovery and preservation of the core. Studies in salt mines also aid in the overall understanding of diapirs (e.g. Burliga, 2014; Schofield et al., 2014; Davison et al., 2017; Warren, 2017), although the focus of mining within the salt itself (rather than overburden) limits their general applicability, while the extractive process could actually enhance and influence fracturing in the overburden.

Recent experimental work by Kaproth et al. (2016) demonstrates that the most significant permeability changes in marine sediments occurs along faults with relatively small magnitudes of displacement. They conclude that “minor faults, which may be difficult to detect in seismic data, may have dramatic implications for reservoir characterization” (Kaproth et al., 2016, p.233). In summary, the geometry, orientation and distribution of fractures may be critical in determining fluid and hydrocarbon flow, and as such are important for both academic and applied studies of salt diapirism (e.g. Archer et al., 2012).

These potential issues from seismic imaging, drill cores and mining through salt structures have resulted in a range of physical modelling studies to better understand salt tectonics. These experiments typically use polymers to represent salt, and either sand (e.g. Koyi et al., 2008; Hudec and Jackson, 2011), mixtures of sand and beads (e.g. Dooley et al., 2015a), silica and garnet sand (e.g. Karam and Mitra, 2016) or glass beads (e.g. Alsop, 1996) as analogues for the deformed overburden. While physical models may offer important information regarding overall deformation around diapiric structures, especially where passively monitored (e.g. Dooley et al., 2015b), they are typically incapable of providing detailed fault and fracture patterns due to scaling issues in granular overburdens.

This study examines fractures and faults developed in overburden around a diapiric salt wall within a strike-slip setting. We use the well-exposed Sedom salt wall that is positioned within the sinistral Dead Sea Fault system as our case study (Figs. 1a, b). This area is ideal as salt (halite) is exposed at the surface within an active, strike-slip plate boundary, thereby removing some of the doubts and variables that develop with analysis of older structures in areas where salt may not be exposed. The area also contains abundant clastic dykes that are formed by injection of over-pressured sediment during seismic events along major faults (e.g. Levi et al., 2006; 2008). Our case study forms the first detailed analysis of fracturing around an exposed halite diapir in a strike-slip setting, and aims to:

i) Analyse overburden fracturing adjacent to the salt diapir;
ii) Describe clastic dykes injected near the salt wall;
iii) Interpret the timing of fracturing relative to drape folding of the overburden;
iv) Discuss the interaction of salt-related fractures with a regional strike-slip fault system.

Our field-based analyses of fault and fracture patterns around this well-exposed salt wall enables us to investigate detailed structural relationships, and thereby evaluate the relative roles of diapirism and regional strike-slip faulting in creating overburden deformation. This study may thus provide a greater appreciation of the likely patterns of fracturing around salt diapirs influenced by regional strike-slip tectonics and has clear implications for hydrocarbons in such settings (e.g. Archer et al., 2012; Jackson and Hudec, 2017, p.336).

2. Geological setting

The Dead Sea Basin is a sinistral pull-apart basin situated between the NNE-trending Dead Sea Western border fault zone (WBFZ) and the Dead Sea eastern border fault (Figs. 1a, b) (e.g. Garfunkel, 1981; Smit et al., 2008a, b; Garfunkel, 2014). A number of faults are developed along the length of the basin, including the sub-surface ~N-S trending Sedom Fault, which displays sinistral strike-slip motion as well as down-throwing towards the deeper basin in the east (Figs. 1b, 2) (e.g. Smit et al., 2008a, b). The Sedom Fault, which separates the ‘intermediate block’ to the west from the deeper basin, is considered to be the major strike-slip fault along the western border of the basin and underlies the Sedom salt wall (Figs. 1b, 2) (Smit et al., 2008a).

The Sedom salt wall is formed of the Sedom Formation predominantly comprising evaporites (75%) including halite, anhydrite and thin dolomites, interbedded with thinner clastics formed of siltstone, mudstone, clay and sandstones (Figs. 3, 4) (Zak, 1967; Frumkin, 2009). The Sedom Formation is subdivided into five members, and incorporates the Bnot Lot Shales Member dated at 6.2 and 5.0 ± 0.5 Ma (Matmon et al., 2014) (Figs. 3, 4). This Late Miocene-Pliocene evaporite sequence penetrates the overlying Plio-Pleistocene Amora Formation and the Late-Pleistocene Lisan Formation that form the exposed overburden to the salt wall, via marginal faults and shear zones (Zak and Freund, 1980; Weinberger et al., 2006b) (Figs. 3, 4). The Amora Formation is subdivided into three members as shown on Figure 4 (Agnon et al., 2006). Although only 400-450 m of Amora Formation are exposed next to the Sedom salt wall, the overall Plio-Pleistocene sequence attains thicknesses of 5500 m in the southern Dead Sea Basin (Al-Zoubi and ten Brink, 2001; Weinberger et al., 2006a). Immediately to the SE of Sedom, the Sedom Deep-1 drill hole penetrated a 3700 m thick fluvio-lacustrine series which overlies a 900 m thick evaporite series (Figs. 1b, 2). To the west of Mount Sedom, the Ami'az East-1 drill hole penetrated a 1300 m thick evaporite series overlain by a 1900 m thick clastic series (Weinberger et al., 2006a) (Figs. 1b, 2). The base of the Lower Amora Member within the Ami'az East-1 borehole has been dated as 3.3±0.9 Ma, while approximately 500 m stratigraphically higher, the Lower Amora beds are dated as 2.7±0.7 Ma (Matmon et al., 2014) (Fig. 4). Overall, the Sedom Formation thickens towards the depocentre in the east and thins towards the western margin of the basin (e.g. Zak, 1967).

The crest of the Sedom salt wall is covered by a 40 m thick caprock, which consists mainly of anhydrite, gypsum, as well as minor marl, clay, dolomite and sandstone fragments. The caprock is considered to have formed from the insoluble material that remained following dissolution of the various salt members (Zak, 1967) during Upper Amora times (340-80 ka) (Zak and Freund, 1980). The late-Pleistocene Lisan Formation overlies the Amora Formation and caprock, and consists of up to 40 m of aragonite-rich and detrital-rich laminae forming a varved lacustrine sequence, dated between ~70 ka and 14 ka by U-series and ^{14}C (Haase-Schramm et al., 2004) (Fig. 4).

3. The Sedom salt wall – an exposed and growing diapir

The Sedom salt wall is a ~10 km long N-S trending ridge that rises ~240 m above the level of the Dead Sea (Figs. 1b, 3). The wall is commonly divided into northern and southern segments, each of which is ~4 km long and ~1.5-2 km wide at surface (Fig. 3). These two segments are separated from one another by a narrower 2 km long central section, where the margins of the wall converge and its width reduces to 800 m (Fig. 3). The western margin of the Sedom wall dips moderately to steeply towards the west, while the eastern flank also dips variably towards the west and is overturned (Weinberger et al., 1997; Alsop et al., 2015). The northern limit of the Sedom salt wall is marked by moderate dips towards the north, where the 'nose' of the salt wall plunges below the surrounding overburden (Fig. 3). Seismic profiles across the salt wall suggest that it is located adjacent to the underlying Sedom Fault, a major ~ N-S trending sinistral-extensional fault that may have focussed the upward flow of salt from depths of 3-4 km (Gardosh et al., 1997; Weinberger et al., 2006a) (Figs. 1b, 2).

N-S trending and west-dipping major normal faults with displacement > 10 m are developed along the western flank of the Sedom salt wall (Fig. 3) (e.g. Zak, 1967; Alsop et al., 2015, 2016a).

The recent active uplift of the salt wall has been largely accomplished via movement on these 'boundary' faults that cut both the Lisan Formation and the salt with its overlying cap rock (Zak and Freund, 1980; Weinberger et al., 2006b; Alsop et al., 2015, 2016a). Upper Amora Member and Lisan Formation that directly overlie the Sedom salt wall represent remnants of a roof that has been carried passively upwards above regional levels by displacement on the boundary faults (Weinberger et al., 2007). The present work focuses on fractures in overburden at greater distances (up to ~ 300 m) from the margins of the salt wall. This analysis of fracturing is largely restricted to the Upper Amora Member and Lisan Formation exposed along the western margin of the salt wall, as the eastern flank is typically obscured by recent (Holocene) sediments and the Dead Sea evaporation ponds (Fig. 3).

Drape folding develops close to the surface where sediments deposited above a growing salt diapir are rotated away from the salt as the diapir moves upwards relative to a subsiding basin (see Giles and Rowan, 2012; Alsop et al., 2016a for summaries). The Sedom salt wall displays broad (>1000 m) areas of upturned bedding that form drape folds, together with withdrawal basins, and angular unconformities defining wedge shaped halokinetic sequences that reflect a phase of dominantly passive diapirism during deposition of the Upper Amora Member (Alsop et al. 2016a). Conversely, during deposition of the overlying Lisan Formation, the Sedom salt wall predominantly displays active diapirism resulting in narrower (<300 m) drape folds and active boundary faults along the margin of the salt wall, which truncate hook-shaped halokinetic sequences and transport them above regional elevations (Alsop et al., 2016a). The Sedom salt wall is not thought to have grown laterally since deposition of Upper Amora Member, as withdrawal basins are still intact around the northern and southern noses of the salt wall (Alsop et al., 2016a).

4. Fracture patterns in overburden around the salt wall

4.1. Overview of bedding and fracture orientations around the Sedom salt wall

Beds within the Upper Amora Member and Lisan Formation dip away from the Sedom salt wall on both its western and eastern flanks (Figs. 3, 5a, b). Deformation within the overburden on the western margin of the salt wall is marked by moderately-steeply dipping NW-SE trending fractures (Figs. 3, 5c, d, e), while fractures within the Upper Amora Member on the eastern side of the salt more generally trend NE-SW (Figs. 3, 5f). Larger faults within the Upper Amora Member and Lisan Formation, that display metres to tens of metres displacement, are typically developed within 300 m of the salt margin (e.g. Fig. 6a-d), although smaller fractures displaying < 1m displacement are also widespread in this area (e.g. Fig. 6e-g). Fractures within both the Upper Amora Member and Lisan Formation are typically extensional and generally form conjugate and domino systems with fractures dipping > 60° towards either the NE or SW (Figs. 5g-o, 6h, i, 7a-o). Overall, although the intensity and spacing of fractures is difficult to quantify due to the lack of flat bedding plane exposures, fracture abundance appears to increase qualitatively towards the Sedom salt wall.

4.2. Orientation of bedding along the western salt margin

The Upper Amora Member and overlying Lisan Formation display a progressive increase in bedding dips when traced towards the western margin of the Sedom salt wall (Figs. 3, 5a, 8a). Increased angles of bedding dip are attributed to syn-depositional drape folding of sediments around the diapir as it rises relative to the sediments (see Alsop et al., 2016a for details). These drape folds are developed on both the western and eastern flanks of the salt wall (Figs. 3, 5b), although they are better displayed on the west due to greater exposure. Moving toward the salt wall, bedding dips start to increase at distances of 1250 m from the western margin of the salt wall within the Upper Amora Member, although the most pronounced increase occurs within 300 m (Figs. 3, 8a). The broad wedge-shaped drape folds within the Upper Amora Member were created during passive diapirism, while the narrower hook-shaped drape fold in the Lisan Formation represent more active diapirism (Fig. 8a) (Alsop et al. 2016a). Adjacent to the Sedom salt wall, the two sequences are separated from one another by an angular unconformity, with the angle of cut-off across the unconformity increasing towards the salt (Fig. 8b).

4.3. Strike and dip of fractures along the western salt margin

Fractures in both the Upper Amora Member and Lisan Formation generally trend NW-SE, and in map view display a progressive clockwise rotation in strike towards the western margin of the salt wall (Figs. 5g-o, 7a, b, 7k-o, 8c-f). At distances of 300 – 200 m from the salt, they have mean strikes of 109° (Lisan Formation) and 127° (Upper Amora Member), while adjacent (<100 m) to the salt they typically strike 144° and 155° respectively (Fig. 5g-o, Table 1). This rotation in fracture trends towards the N-S trending salt wall is summarised in a series of rose diagrams (Fig. 9) and a schematic map (Fig. 10a) that present subsets of fracture data from greater distances (300 m -200 m, Fig. 9a, b; 200 m – 100 m, Fig. 9c, d) to closer to the salt wall (0 – 100 m, Fig. 9e, f).

At any given distance from the salt margin, the fractures in the Upper Amora Member typically strike clockwise of those fractures in the overlying Lisan Formation (Fig. 8e, f, 9a-f, 10a). This is also illustrated when fracture strikes are compared to the dip of bedding, with steeper bedding in the Upper Amora Member closer to the salt reflecting upturn over a more protracted interval (Fig. 8g, h). In addition, fractures developed within both the Upper Amora Member and Lisan Formation in the southern Sedom salt wall are marginally more clockwise than those adjacent to the northern portion (Fig. 8f). This relationship mirrors the overall bend in the Sedom salt wall, with the southern segment trending ~20° clockwise of the northern salt wall (Fig. 3). Rose diagrams of overall fault trends (Fig. 9a-f) display a bimodal tendency, which reflects the different strikes of NE and SW dipping extensional faults (Fig. 8e, f) together with the slight bend in the northern and southern segments of the salt wall (Figs. 3, 5g-o).

The ~30° clockwise rotation of mean fracture strikes towards the salt (Fig. 9a-f, 10a) is also marked by fracture dips becoming steeper nearer the salt (Fig. 5g-o, 8i, 10b). Considerable ‘scatter’ exists in the dip of fracture planes compared to distance from the salt margin, although fractures typically get steeper to sub-vertical (~70°-80°) nearer the salt (Fig. 8i, 10b). Within ~50 m of the salt, some east-dipping fractures in both the Upper Amora Member and Lisan Formation become less steeply dipping (~65°) (Figs. 8i, 10b).

4.4. Strike and dip of fractures around the nose of the salt wall

Further constraints on fracture controls and timing are provided by measuring the orientation of fractures within the Upper Amora Member exposed around the lateral terminations or ‘nose’ of the salt wall. Overburden around the northern nose is better exposed than that at the southern termination, with moderately NW-dipping bedding containing a conjugate system of NW-SE and NNE-SSW trending extensional fractures (Fig. 3, 7c, d, e). On the NW side of the nose, bedding dips moderately towards the NW and conjugate fractures trend NW-SE (Fig. 3, 7c), while on the NE side, the bedding dips moderately-gently towards the NE and conjugate fractures trend NNE-

SSW (Fig. 3, 7e). The conjugate fractures collectively fan around the northern nose, and this pattern is mirrored at the southern nose, although it is less clear due to relatively poor exposure of the overburden (Fig. 7i, j, k).

4.5. Strike and dip of fractures along the eastern salt margin

Although overburden along the eastern margin of the Sedom salt wall is poorly exposed due to recent alluvium and Dead Sea evaporation ponds, it does provide useful information about overall fracture patterns around the diapir as a whole (Figs. 5f, 7f, g, h). The Lisan Formation is nowhere exposed along this eastern contact, and overburden consists entirely of Lower and Upper Amora Member separated by the intervening Amora Salt Member (Figs. 3, 4). Along the eastern flank of the salt wall, bedding in the Upper Amora Member dips moderately-steeply eastward (and may locally become overturned) (Figs. 3, 5b), while fractures trend NNW-SSE and NE-SW (Figs. 3, 5f, 7f, g, h). Where fracture orientations in the Lower and Upper Amora Members were collected adjacent to one another, the fractures in the Upper Amora Member strike marginally clockwise to those in the Lower Amora Member (Fig. 7g), although the two populations do overlap.

5. Nature and timing of fractures in overburden around the salt wall

5.1. Extensional fractures in the overburden

Conjugate (e.g. Fig. 11a, b) and domino-type (e.g. Fig. 11c, d, e) fracture systems are developed throughout the Upper Amora Member and Lisan formations adjacent to the Sedom salt wall (Figs. 6a-i, 7a-o, 11a-e). NW-SE trending extensional fractures dip at angles of ~60° and define conjugate patterns in both the Upper Amora Member and Lisan Formation (Figs. 6a-i, 7a-o, 11a, b). Most conjugates form intersections plunging broadly in the dip direction of bedding (Figs. 6h, i, 11a, b), suggesting that the greatest stretching of beds is parallel to their strike along the N-S length of the Sedom salt wall.

5.2. Age of fractures in the overburden

Fractures cutting poorly lithified sediments rarely preserve slickensides, but those lineations that were observed indicate normal dip-slip motion down the fault plane and also suggest a degree of lithification within the Upper Amora Member at the time of faulting (Fig. 11f). However, conglomerate layers are ‘smeared’ along faults within the Upper Amora Member, suggesting in this case that the matrix to these units was not fully lithified at the time of faulting (Fig. 11g). Some conjugate fractures do not meet at a lower ‘point’, but rather are accommodated in underlying beds of sand that undergo thinning and are able to flow to assist extension and dilation (e.g. Morley, 2014) (e.g. Fig. 11i). These relationships support the ‘soft-sediment’ nature of deformation adjacent to the salt, and suggest that the fractures formed early rather than later in the tectonic history. Faults cut through entire slumped horizons within the Lisan Formation (e.g. Fig. 11h), suggesting that they do not relate to regional slumping and development of mass transport deposits (e.g. Alsop and Marco, 2014; Alsop et al., 2016b; 2017), but rather stretching of beds as they accommodate subsequent diapir movement. In summary, some faults preserve slickensides and cut through entire sequences, suggesting they formed relatively ‘late’. Other fractures preserve ‘soft-sediment’ smearing of conglomerates, flow within sandstone, and hangingwall ‘growth’ sequences (e.g. Fig. 6g) indicating faults were ‘early’ and syn-depositional (Alsop et al., 2016a).

5.3. Clastic dykes in the overburden

Clastic dykes formed by injection of overpressured sediment are developed over large parts of the Ami'az Plain (Levi et al., 2006, 2008, 2011) where they typically define mode 1 (opening) fractures (Fig. 7a). The clastic dykes apparently propagated at velocities of tens of metres per second and at pressures of 1-10 MPa (Levi et al., 2008). They appear to be restricted to the Lisan Formation, where they act as markers to define horizontal displacement during coseismic deformation (Weinberger et al., 2016). Clastic dykes are also well developed in the Lisan Formation near the western margin of the narrower central part of the Sedom salt wall (around Grid 23635550, see Fig. 3), where they are typically between 5 cm and 20 cm thick, and can form intense networks of injected dykes that display branching geometries (Fig. 12a-e). In plan view, the clastic dykes typically define linear intersections on bedding planes (Fig. 12d). Adjacent to the diapir, they are frequently marked by extensional offset of bedding, suggesting shear fractures rather than mode 1 opening as observed on the Ami'az Plain (Levi et al., 2006, 2008) (Fig. 12b-e). The lack of sedimentary growth geometries on fractures filled by clastic dykes indicates that they did not simply utilise and infill older syn-sedimentary faults. Clastic dykes injected along fractures are typically NW-SE to N-S trending, dip at angles of >60° and may intrude along both domino and conjugate extensional faults (Fig. 12f-j). The injection of clastic dykes suggests high fluid pressures associated with hydraulic fracturing.

5.4. Gypsum veins in the overburden

Gypsum veins are more abundant towards the margin of the salt wall in both the Upper Amora Member and Lisan Formation, but are largely absent at greater distances (> 300 m) from the salt contact, apart from very locally within some mass transport deposits (Alsop et al., 2017). Within ~50 m of the Sedom salt wall, the overburden is intensely fractured and contains significant amounts of gypsum net-veining (Fig. 13a, b, c) (see also Alsop et al., 2015, their fig. 9). Gypsum-filled fractures form NW-SE trending conjugate systems of similar orientation to previously described faults and clastic dykes. (Fig. 13c, d, e). They are up to 3 cm thick, and commonly develop parallel to bedding planes with steep fibres suggesting sub-vertical 'jacking open' of the fractures via high fluid pressures (see Davison et al., 1996b; Alsop et al., 2015 their fig. 9f) (Fig. 13f, g). We find no evidence that the currently observed gypsum veins initiated as early anhydrite that subsequently underwent hydration and 30-67% volume increase as they transformed into gypsum (see Warren 2016 p. 667 for details of the process). All observed veins contain gypsum (without anhydrite), and no hydration-induced folds linked to the potential volume increase are seen in the finely-laminated Lisan Formation near the gypsum veins. Thus, clastic dykes coupled with gypsum vein complexes indicating vertical 'jacking-up' of overburden collectively suggest that high fluid pressures were locally developed around the salt wall.

5.5. Contractional faults in the overburden

Despite the Sedom salt wall undergoing a recent phase of active diapirism since 14 ka (e.g. Weinberger et al., 2007; Alsop et al., 2016a), evidence for contractional faulting in the overburden is very limited (Fig. 14a). Within the Lisan Formation, rare NE-SW striking and moderately (~45°) SE-dipping reverse faults displace bedding by ~ 10 cm (Fig. 14a-e). The observation that reverse faults also cut slumped horizons, and displace the hangingwall towards the NW in a direction opposite to the general slump direction (e.g. Alsop and Marco, 2012a, b) indicates that reverse faults do not relate to mass transport events within the Lisan Formation. Reverse faults are locally cut by clastic dykes, demonstrating that reverse faulting is not a younger event and is broadly of the same age as extensional faulting (Fig. 14d, e). Clastic dykes may display extensional offsets of bedding and the earlier thrusts (Fig. 14d, e). The strike of reverse faulting (047º) (Fig. 14b) is orthogonal to the trend of local extensional fractures on the western flank of the salt wall (Fig. 5n, o).

6. Discussion

6.1 Overburden fracturing adjacent to a salt diapir

Outcrop studies have previously suggested that small-scale deformation in the sedimentary overburden around salt diapirs is relatively insignificant (e.g. Rowan et al. 2003, p.737). Indeed, the role of smaller faults and fractures in the development of drape folds around salt diapirs is typically not discussed in detail (e.g. Giles and Rowan, 2012; Ringenbach 2013). Perhaps, this approach is a consequence of salt being considered weaker than surrounding sediments and therefore capable of absorbing deformation (e.g. Schultz-Ela, 2003, p. 760), while smaller faults are difficult to image on seismic sections. Hearon et al. (2015a, p203) working on outcrops of Neoproterozoic strata in south Australia noted that even below the remains of salt sheets "no small-scale subsalt deformation such as shearing, fracturing or pervasive faulting is present" while Rowan et al. (2016, p.1741.) described the upturned sequences next to the same diapirs as containing "almost no small-scale faulting". Working on Albian-aged diapirs in the Pyrenees, Poprawski (2014, p.763) recorded that "most of faults affecting the overburden are related to regional tectonics and not to diapir growth". However, recent analysis of magnetic fabrics around these Pyrenean diapirs by Soto et al. (2017) suggests that diapir-related deformation may locally be preserved within the overburden. Likewise, numerical modelling undertaken by Nikolinalou et al., (2017) indicates that significant shear strains and deformation may indeed develop within upturned sediments around the flanks of salt diapirs.

The question arises as to whether drape folds developed in unlithified sediments are indeed capable of developing brittle faults and fractures, as suggested by Alsop et al. (2000) for Carboniferous-aged diapirs in Nova Scotia (see also Vargas-Meleza et al., 2015). This problem is non-trivial as small faults and fractures may be crucial for fluid and hydrocarbon migration (e.g. Kaproth et al., 2016). In an attempt to answer this question and provide some 'ground-truthing' for numerical models of overburden deformation (e.g. Nikolinalou et al., 2017), we have tried to isolate the influence of the salt diapirism from regional tectonic faults such as the Sedom Fault that underlies the diapir (Figs. 1b, 2).

Firstly, we have examined the nature of the Lisan Formation adjacent to the regional western border fault zone (WBFZ) just 5 km further west (Grid 23245551), and along which no salt diapirs are present (Fig. 1b). After detailed field examination, we report that no enhanced fracturing has been observed within the Lisan Formation adjacent to the WBFZ (Figs. 1b). Although this absence of evidence is not conclusive, as it could be argued that this portion of the WBFZ was simply not active during or after deposition of the Lisan Formation, it suggests that at least some of the observed fractures near to the Sedom salt wall are generated by salt emplacement rather than regional tectonics.

Secondly, we examined the Upper Amora Member and Lisan Formation that lie above the continuation of the subsurface Sedom Fault beyond the northern and southern terminations of the Sedom salt wall. Once again, we report that no enhanced fracturing was observed along the projected surface trace of the fault beyond where the salt is exposed. In addition, the Sedom Fault is developed adjacent to the Sedom salt wall only in the central narrow section, and then deviates away from the salt wall to the north and south (Figs. 1b, 3). However, fractures are developed all the way along both the western and eastern salt margins and also around the northern nose of the salt wall (Fig. 7), thereby suggesting that the salt wall mainly controls fracturing.

Thirdly, clastic dykes with notable extensional offset and gypsum veins were only recorded adjacent to the exposed salt and are not observed along the WBFZ (e.g. Figs. 12, 13). However, injected clastic dykes are best developed in the Lisan Formation near the narrower central area of the salt wall where the subsurface Sedom Fault is interpreted to be close to the salt (Figs. 1b, 3).

Fourthly, the width of upturned bedding associated with drape folds extends for greater distances from the western Sedom salt wall into the Upper Amora Member than in the overlying Lisan Formation (Alsop et al., 2016a) (Figs. 5a, 8a, b). The fracture trends in the Upper Amora Member are clockwise to those in the Lisan Formation and this obliquity, which ranges across the entire upturned area, becomes more pronounced at greater distances from the Sedom salt wall (Figs. 5m, n, o, 9a-f, 10a). As the underlying and steeply dipping Sedom Fault is at an equivalent distance to both the Upper Amora Member and Lisan Formation, it is difficult to link variable fracture trends to the Sedom Fault itself. However, if fracturing partially occurred during upturning of beds then any obliquity in fracture trends simply reflects the greater amounts of upturn in the Upper Amora Member compared to the Lisan Formation at any given distance from the salt wall (Fig. 8g, h).

In summary, our observations collectively suggest that at least a significant component of fracturing is related to drape folding associated with salt diapirism (Fig. 10a, b). This conclusion differs from those of Hearon et al. (2014; 2015b), Poprawski (2014), and Rowan et al. (2016), who all suggest that little or no faulting relates to salt diapirism and drape folding. Our observations of the fracture population adjacent to the Sedom salt wall may reflect: a) the nature of the lithologies together with the rapid rates of salt movement and uplift along the Sedom salt wall that are estimated at ~ 5 mm per year (Alsop et al. 2016a; Weinberger et al., 2007); b) superb quality of outcrop that permits detailed observations along the actively rising diapir; c) absence of any later regional contractional overprint, which would have possibly masked diapir-related fractures in studies of older diapirs; and d) the linear geometry of salt walls may encourage greater fracturing than typically observed around circular salt stocks.

6.2. Clastic dykes injected near a salt wall

The injection of clastic dykes along extensional fractures that share similar orientations and kinematics to faults observed along the entire western flank of the Sedom salt wall suggests that some clastic dykes relate to the Sedom salt wall (Fig. 12f-j). However, the prevalence of clastic dykes near the narrower central section of the salt wall, where the subsurface Sedom Fault is adjacent to the salt, suggests that some clastic injections may be created by seismicity along this underlying fault. This interpretation is supported by the ‘branching geometry’ of injected clastic dykes (Fig. 12d, e) and their spacing density (Fig. 12c-e) that implies high fracture and injection velocities (Levi et al., 2008). Although clastic dykes are capable of being intruded in areas of contraction (e.g. Palladino et al., 2016), they more typically inject in areas undergoing extension, such as represented by normal faults near the Sedom salt wall.

Optically stimulated luminescence (OSL) ages of quartz from within the clastic dykes on the Ami’az Plain give ages of between 15 and 7 ka (Porat et al., 2007), which post-dates deposition of the 70-15 ka Lisan Formation (Haase-Schramm et al., 2004). Clastic dykes intruded along extensional faults adjacent to the Sedom salt wall are also younger than the Lisan Formation, and possibly relate to boundary faults that cut caprock developed above the salt wall (e.g. Zak, 1967, Alsop et al., 2016a). In summary, we interpret the clastic dykes near the western margin of the Sedom salt wall as being created by fluidisation and injection of over-pressured sediment along hydraulic fractures, potentially linked to seismicity and movement along the underlying Sedom Fault. A further implication of these clastic dykes centred near to, and directly above salt, is that the largely unconsolidated sediment within dykes forms easily erodible conduits, resulting in crevasses that would facilitate overall break-up and 'spalling' of overburden blocks off the growing salt wall.

6.3. Timing of fracturing relative to drape folding of the overburden

Having established that a significant portion of the fracturing history is coeval with the diapiric rise of salt (see section 6.1. above), we now consider the relative age relationships between drape folding and fracturing.

6.3.1. Could fractures develop before drape folding?

Extensional faults display sedimentary growth geometries in both the Upper Amora Member deposited between 340 – 80 ka (Torfstein et al., 2009) and also the younger Lisan Formation deposited between 70 – 14 ka by U-series and ^{14}C (Haase-Schramm et al., 2004), and therefore are clearly syn-depositional (see also Alsop et al., 2016a) (e.g. Fig. 6g). Such growth faults would then undergo a component of rotation as beds are subsequently tilted into drape folds (Alsop et al., 2016a) (Fig. 15a). However, the majority of east-dipping fractures developed at 200-300 m from the salt margin do not display growth geometries and become more steeply dipping at distances of 100-200 m from the salt (Figs. 8i, 10b). Notably, any early fractures dipping eastwards would be expected to dip more shallowly east (< 30°) if they were rotated along with bedding nearer the salt (Figs. 8a, 15a). Conversely, original west-dipping extensional fractures could rotate through the vertical to become east-dipping faults with apparent thrust sense (Fig. 15a). Such relationships are not observed along the flanks of the Sedom Salt wall.

In summary, faults do not display a distinct or simple linear pattern of changing dips with increased tilt of bedding in drape folds (Fig. 8j, 10b), suggesting no overall rotation of faults. Thus, although some fractures are early and syn-depositional with respect to the Upper Amora Member and Lisan Formation, most fractures would appear to be later and do not develop before drape folding of beds.

6.3.2. Could fractures develop after drape folding?

Faults and fractures that developed late in the deformation history following the creation of drape folds might be expected to have an overprint of reasonably constant orientations across the zone of upturned bedding (Fig. 15b). However, our data demonstrate a distinct and systematic increase in fracture dips and strikes towards the salt (Figs. 8, 9a-f, 10a, b). Within 50 m of the salt, east-dipping extensional faults within both the Upper Amora Member and Lisan Formation locally dip at 60°-65° (Fig. 8i), which is the angle that fractures preserve in the outer (> 250 m) parts of the drape fold (Fig. 10b). This consistency suggests that some fractures immediately adjacent to the salt may form relatively late and be superimposed on upturned bedding (Fig. 15b). Although it could be argued that variably orientated bedding played a mechanical role and locally influenced fracture orientation, we believe this to be unlikely as sediments are exceptionally weak and were largely unlithified or, at best, very poorly lithified at the time of deformation. The Upper Amora Member remains very poorly lithified while the Lisan Formation still contains 25% water and is largely unlithified (Arkin and Michaeli, 1986). Therefore, the systematic variations in fracture patterns are inconsistent with a deformation history where fractures were universally superimposed on the drape folded units at a late stage, and we discount that possibility.

6.3.3. Could fractures develop during drape folding?

The development of fractures during drape folding adjacent to the Sedom salt wall is broadly supported by the first-order observation that the zone of fracturing is largely restricted to, and coincides with the extent of drape folding (Figs. 3, 8a, c, 10a, b, 15c). Adjacent to the Sedom salt wall, fracture strike and dip vary appreciably within both the Upper Amora Member and Lisan Formations as the salt contact is approached (Figs. 5g-o, 8a-j, 9a-f, 10a, b). Fractures typically strike NW-SE and dip towards both the NE and SW, generally at angles >60° (Figs. 5, 7, 8, 9a-f, 10a, b). However, most fracture data is collected within 250 m of the salt margin, which is the point where more marked upturn of the bedding commences to define drape folds (Alsop et al., 2016a). In addition, the intensity of fracturing qualitatively increases as bedding dip increases, although clearly different lithologies may also influence this general pattern. The observation that fracture trends systematically vary as bedding dips increase towards the salt is consistent with fractures forming during rotation and upturn of beds into drape folds (Figs. 5, 8g, h, 15c). As might be expected, steeper bedding dips in the Upper Amora Member are associated with more clockwise trending fractures when compared to the overlying Lisan Formation (Figs. 5m, n, o, 8g, h). The general increase in fracture dip and intensity towards the salt wall is consistent with fractures accommodating some of the bedding rotation during drape folding (Fig. 10b, 15c). Our observations collectively suggest that a significant proportion of fractures developed around the entire Sedom salt wall during drape folding, rather than before or after it. However, we cannot exclude the possibility that at least some fractures initiated pre-rotation and were associated with growth faulting, while others are post-rotation and link to continued movement on boundary faults or the underlying Sedom Fault.

6.3.4. Protracted fracturing within older drape folded sequences

Within the Upper Amora Member, it is not generally possible to separate fractures which formed during the older passive phase of diapirism from those which are younger and formed during the subsequent active phase of diapirism associated with deposition of the overlying Lisan Formation. Exceptions to this issue include some extensional faults that are clearly cut by the unconformity at the base of the Lisan Formation, while other faults displace this unconformity and must therefore be younger (Alsop et al., 2016a). However, fractures in the Upper Amora Member collectively display more variable patterns suggesting that they may have a more protracted history, including being affected by younger fractures associated with active diapirism (Alsop et al., 2016a). Older fractures formed during drape folding of the Upper Amora Member would, together with bedding, be subsequently rotated further during active diapirism. This possibility is clearly illustrated by examining the angle of cut-off preserved within the Upper Amora Member across the base Lisan unconformity (Figs. 8a, b, 10b). At distances of 250 m from the salt, cut-off angles of 20° are preserved along the base Lisan unconformity (Fig. 8b), suggesting that the underlying syn-Upper Amora Member fractures will also rotate by this amount prior to deposition of the overlying Lisan

Formation. However, observed angles of fracture may display significantly less variation than this (Fig. 8i, j), as the strike of mean fractures in the Upper Amora Member at this distance is 120°, which is only 30° oblique to the direction of rotation along the N-S trending salt wall in map view (i.e. steep faults parallel to the direction of rotation will simply tend to rotate within their own plane). In summary, some faults and fractures are early because they have growth geometries and/or are cut by the base Lisan unconformity, whereas others are relatively late as they cut and displace this unconformity or are infilled by clastic dykes dated at 15-7 ka (Porat et al., 2007).

6.4. Interaction of salt-related fractures with a regional strike-slip fault system

The role of strike-slip faulting in salt tectonics was recently summarised by Jackson and Hudec (2017, p.336) who highlight the importance of diapir timing relative to thick-skinned (whole-crustal) or thin-skinned strike-slip tectonics. Within the study area, the crustal-scale Dead Sea Fault system is thick-skinned and initiated during the early Miocene (Nuriel et al., 2017), while diapirism associated with the Sedom salt wall did not commence until the Plio?-Pleistocene when the Amora Formation was deposited over the Sedom Formation and then around the growing salt diapir (Figs 3, 4) (Weinberger et al., 2006; Alsop et al., 2016a).

Fracture trends measured in map view from the southern portion of the Sedom salt wall are marginally clockwise of those measured in the north, because the contact of the Sedom salt wall is also orientated slightly clockwise (Figs. 3, 5g-l, 8f). Overall, the Sedom salt wall has a 'banana' shape in map view, with the southern segment trending clockwise of the northern portion. This geometry could reflect a gentle curvature in the underlying Sedom Fault (Fig. 1b), with the concave to the west geometry resulting in a 'pull-apart' during sinistral motion. Alternatively, the Sedom Fault could be segmented with left-stepping faults leading to a pull-apart between them. The source of a suggested extrusive salt flow from the Sedom salt wall at 420 ka (Alsop et al., 2015) is located in this potential pull-apart along the Sedom Fault strands. Similar models of extrusive salt flows emanating from pull-aparts have been proposed for Iranian salt glaciers by Talbot and Aftabi (2004). In addition, injected clastic dykes with extensional offsets and branching geometries (Fig. 12a-j) are also developed in this central area of the Sedom salt wall. They may reflect high velocity intrusion and failure associated with seismicity and tensional 'wing cracks' (see Fossen, 2016, p.406) developed from the terminations of underlying step-over strands.

On a more regional scale, the N-S trending Sedom salt wall forms in a transtensional pull-apart jog within the overall NNE-SSW trending sinistral Dead Sea Fault system (e.g. Smit et al., 2008a, b). Larsen et al (2002) suggested that the N-S trending Sedom Fault has undergone sinistral strike-slip tectonics as well as extensional motions that downthrow toward the deeper basin in the east (Figs. 1b, 16). Subsequently, Smit et al. (2008a, p.6) even suggested that the Sedom Fault "is the main strike-slip fault along the western border of the basin". It is the obliquity of this N-S trending strike-slip fault relative to the major strike-slip discontinuity marking the NNE-trending Dead Sea Fault system that creates increased horizontal extension and diapirism above the Sedom Fault (Smit et al., 2008a, p.11) (Fig. 16).

The laboratory experiments of Smit et al. (2008a, b, 2010) and Brun and Fort (2008) suggest that above the intermediate block to the west of the Sedom Fault, the overburden is still 'coupled' to the underlying basement due to the salt being thinner than in the deeper basin (Smit et al. 2008a, p.11) (Figs. 1b, 2, 16). This coupling allows the overburden to be subjected to simple shear associated with basement-driven sinistral strike-slip deformation, and results in NW-SE trending normal faults developed perpendicular to the λ1 principal stretching direction in the overburden (Smit et al., 2008a their fig. 13b). These oblique normal faults formed at later stages of deformation with an obliquity of ~45° to the shear direction (Smit et al., 2008a, p.13). Our detailed fracture analysis in the study area supports this model-based interpretation (Figs. 5, 7, 9, 16). Contractional reverse faults are modelled by Smit et al. (2008a) to develop normal to the principal shortening direction (λ3) and would trend NE-SW, which we also confirm for the small population of reverse faults that we found and characterised (Figs. 14, 16).

The presence of the ductile salt layer results in more distributed strike-slip deformation in the overlying overburden. Consequently, contractional and extensional deformation affects wider zones in the overburden above the salt, with continuing strike-slip deformation resulting in rotation of extensional structures thereby leading to 'sigmoidal' traces that curve toward the shear direction in map view (Smit et al., 2008a, p.13; see also Dooley and Schreurs, 2012). This swing in extensional fracture trends is clearly recorded in the present study (Figs. 5g-i, 8, 9, 10a, 16).

In summary, the rare NE-SW trending reverse faults, together with the NW-SE striking normal faults that collectively rotate towards more NNW-SSE orientations in the overburden adjacent to the Sedom salt wall largely confirm and support the modelling of Smit et al. (2008a, b). The overall distribution of fractures adjacent to the Sedom salt wall indicates that they are associated with upturn of bedding and drape folding, while the orientation and systematic rotation of extensional fracture trends indicates that they are also linked to regional strike-slip tectonics along the Sedom Fault. Smit et al. (2008a, p. 12, their fig. 11) show from modelling that such extensional fractures may develop sigmoidal shapes in map view where they rotate towards major strike-slip faults bounding elongate diapirs or walls, and collectively "indicate N-S stretching in this area" (Smit et al., 2008a, p.10). We therefore have two competing influences on the generation of small faults and fractures in overburden linked to a) diapiric processes associated with the upturn of bedding and development of drape folds around the Sedom salt wall, and b) regional tectonic processes associated with the sinistral Sedom Fault that underlies the salt wall. This results in a 'mixed pattern' of fractures that has developed over a protracted period of time during both passive and active growth of the salt wall.

7. Conclusions

The development of overburden fractures within upturned bedding on both the western and eastern margins of the diapiric Sedom salt wall demonstrates that fracturing is a significant and integral process during drape folding. Zones of intense minor faulting and fracturing that are spatially restricted to the lateral margins and nose of the salt wall, may reflect the rapid rise of salt at rates of ~ 5 mm / year (see Alsop et al., 2016a; Weinberger et al., 2007), combined with the elongate shape of the salt wall. Fractures display a range of age relationships relative to bedding upturn, with growth faults demonstrating that some faults initiated during deposition of sediments prior to rotation of beds to form drape folds. However, evidence for systematic rotation of fractures as bedding dips increase towards the salt is absent, suggesting that many fractures actually form during drape folding and helped accommodate rotation of strata. Fracture orientations in older units display greater scatter due to their more prolonged history of upturn, and also potential reactivation of these faults during later active diapirism.

Fractures within the overburden do not define a simple radial and circumferential map pattern relative to the Sedom salt wall. In map view, fractures fan around the northern nose of the salt wall and also maintain high angles to the eastern salt margin to define a semi-radial fracture pattern. However, the western flank of the salt wall is marked by a clockwise rotation of fractures towards the salt, suggesting that diapir-related fractures within drape folds formed in a stress field that was the result of the interaction of the stresses generated by diapir emplacement with stresses due to regional strike-slip faulting to create 'mixed' fracture patterns. Here, the 45° anticlockwise obliquity of overburden fractures relative to the N-S trending salt wall is consistent with transtensional deformation along the sinistral Sedom Fault that underlies the salt wall (Fig. 16). The prevalence of branching injected clastic dykes near the narrow central portion of the salt wall that is closest to the underlying Sedom Fault suggests that seismicity along this fault could also lead to sediment injection. The presence of these clastic dykes, together with bedding-parallel gypsum veins that 'jack-up' the overburden, demonstrates that high fluid pressures were locally attained next to the salt wall.

This field-based study has demonstrated a clear link between salt diapirism and strike-slip faulting in terms of both of them simultaneously affecting the stress field in the rock volume of the study area. Furthermore, the relationship between overburden fracturing and upturn of bedding next to a salt diapir has a number of implications regarding the role of fracturing and mechanics of drape folding. Based on our observations, we suggest that salt does not necessarily accommodate all of the shearing along the diapiric margin (cf. Shultz-Ela, 2003), and that significant deformation may be accommodated via fracturing within the overburden itself. The exact nature and inter-layering of the overburden (lithology, degree of lithification, presence of fluids etc.) coupled with the types of salt (halite, carnallite etc.) and rates of diapiric movement will all influence the resulting styles of deformation. The presence of faults and fractures that potentially segment and compartmentalise drape folds has broader implications for hydrocarbon exploration next to salt diapirs, and suggests that deformation in overburden next to salt cannot be simply pigeon-holed into 'end-member' scenarios of purely brittle faulting or viscous flow.

Acknowledgements

RW was supported by the Israel Science Foundation (ISF grant No. 868/17). SM acknowledges the Israel Science Foundation (ISF grant No. 1436/14) and the Ministry of National Infrastructures, Energy and Water Resources (grant #214-17-027). We would like to thank reviewers Chris Talbot and Tim Dooley for careful and constructive reviews, together with Bill Dunne for efficient editorial handling.

Figures

Fig. 1 a) Tectonic plates in the Middle East. General tectonic map showing the location of the present Dead Sea Fault (DSF). The DSF is a left-lateral fault between the Arabian and African (Sinai) plates that transfers the opening motion in the Red Sea to the Taurus – Zagros collision zone with the Eurasian plate. Location of b) shown by the small box on the DSF. b) Map of the Dead Sea showing the position of the exposed Sedom salt wall and strands of the Dead Sea Fault (based on Sneh and Weinberger, 2014). The locations of the RV-7003 seismic line (Fig. 2), together with the Sedom Deep-1 and Ami'az East-1 boreholes are shown, as is the subsurface trace of the Sedom Fault.

Fig. 2. Time-migrated interpreted seismic profile RV-7003 across the Sedom salt diapir and adjacent overburden sediments (from Weinberger et al., 2006a). The seismic highlights the position of the sub-surface

Sedom Fault that is considered to have controlled the location of the Sedom salt wall, and divides the Dead Sea Basin into intermediate and deep blocks. The underlying source layer of salt (Sedom Fm.) is traced across the Sedom Fault, where it drops down into the deep block marked by much greater overburden thicknesses. The locations of the RV-7003 seismic line, together with the Sedom Deep-1 and Amiaz East-1 boreholes that constrain overburden thicknesses are shown in Figure 1b.

Fig. 3 Geological map of the Sedom salt wall and adjacent sedimentary overburden based on Zak (1967) and Agnon et al. (2006). The orientations of extensional fractures within the overburden are shown. The location of the NW and SW Sedom subareas along Northing 555 are highlighted. See Figure 1b for location.

Fig. 4 Generalised stratigraphy and ages of the Sedom Formation that comprises the Sedom salt wall, and the Amora and Lisan Formations that form the overburden to the salt. Note that dissolution of salt members leads to local caprocks being preserved at the surface. TCN – Terrestrial cosmogenic nuclide burial ages.

Fig. 5 Stereonets of bedding from the a) western margin of the Sedom salt wall, and b) eastern margin of the salt wall. c) Stereonets of fractures from the western margin of the salt wall are separated into d) fractures within the Lisan Formation, e) fractures within the Upper Amora Member (UAM). f) Fracture orientations from the Upper Amora Member along the eastern margin of the Sedom salt wall. g- l) Stereonets of extensional fractures in Upper Amora Member and Lisan Formation measured at distances of 300-200 m, 200-100 m, and 100-0 m from the western margin of the Sedom salt wall. Data are subdivided into NW Sedom (g-i) and SW Sedom (j-l) domains that are north and south of Grid Northing 555 respectively (see Fig. 3 for boundary, Table 1 for exact numbers of fractures in each unit). m-o) Summary stereonets of mean fractures that combine both NW and SW Sedom data sets. Data from the Lisan Formation are shown in orange, with poles to NE dipping fractures (diamonds) and SW dipping fractures (squares). Data from the Upper Amora Member are shown in brown, with poles to NE dipping fractures (circles) and SW dipping fractures (triangles). In each case, the calculated mean fracture plane is shown by the orange (Lisan Formation) and brown (Upper Amora Member) great circles. In m-o), mean bedding in the tilted Upper Amora Member and Lisan Formation are also shown by the brown and orange dashed great circles respectively.

Fig. 6 a-f) Photographs of larger faults at outcrop scale within the Upper Amora Member and Lisan Formation. g) Photograph of ‘growth’ fault within the Lisan Formation. h) Photograph and associated stereonet (i) of conjugate extensional fractures in the Upper Amora Member. Data on stereonet i) is represented by: bedding (red great circles and poles by solid red squares), fractures (blue great circles and poles by solid blue circles), mean intersection of conjugate fractures (open blue circle).

Fig. 7 Examples of representative structural data collected from individual sites within the Upper Amora Member around the Sedom salt wall (a). Data on stereonets b-o) are represented by: poles to bedding (solid red squares), mean bedding (open red square and red great circle), poles to fractures (solid blue circles), mean fractures (open blue squares and blue great circles). Fractures that form conjugates dipping in opposing directions are distinguished by separate means. In g), poles to fractures measured in the Lower Amora Member are shown by blue triangles, while those in the Upper Amora Member are represented by blue circles.

Fig. 8 Graphs showing relationships between extensional fractures and bedding adjacent to the western margin of the Sedom salt wall. a) Distance to salt margin compared with the dip of beds in the Upper Amora Member (N=104) and Lisan Formation (N=56). b) Distance to the salt margin compared with the angular obliquity of beds across the unconformity at the base of the Lisan Formation. ‘Best-fit’ curves on graphs a) and b) illustrate general trends. Distance to the salt margin is compared with the strike of fractures in c) Upper Amora Member (N=151), and d) Lisan Formation (N=133). In graphs e - j), mean data was calculated for each 50 m wide ‘zone’ measured as a distance from the western salt margin. e) Distance to salt margin compared with the mean strike of west and east-dipping fractures, while f) shows this data separated into NW and SW Sedom sub areas that are north and south of Grid Northing 555 respectively (see Fig. 3). g) Mean dip of bedding compared with the mean strike of west and east-dipping fractures, while h) shows this data separated into NW and SW Sedom sub areas. i) Distance to salt margin compared with the mean dip of west and east-dipping fractures. j) Mean dip of bedding compared with mean dip of west and east-dipping fractures.

Fig. 9 Rose diagrams with 10° petals displaying fracture trends in the Upper Amora Member (UAM) and Lisan Formation measured at (a, b), 300-200 m, (c, d) 200-100 m and (e, f) 100-0 m from the western margin of the Sedom salt wall (see Fig. 5 and Table 1). Mean fracture trends (large arrows) are clockwise in the UAM as compared to the Lisan Formation. Fracture trends in both units display an overall clockwise rotation towards the western margin of the Sedom salt wall.

Fig. 10 a) Schematic synoptic map of fracture trends, and b) cross section summarising fracture dip angles from the Upper Amora Member (UAM) (shown in brown) and Lisan Formation (shown in orange) exposed along the entire western flank of the Sedom salt wall. Fracture data represent means from each interval measured at set distances (300 – 200 m etc.) from the salt wall.

Fig. 11 Photograph a) and associated stereonet b) show conjugate extensional fractures within the Upper Amora Member, while photograph c) and associated stereonet d) shows domino faulting within the Upper Amora Member. Data on stereonets b, d) is represented by: bedding (red great circles and poles by solid red squares), fractures (blue great circles and poles by solid blue circles), mean intersection of conjugate fractures (open blue circle). e) Domino-style fractures within the Lisan Formation. f) Dip-slip slickenslides on a fault plane cutting the Upper Amora Member. g) Conglomerates smeared along an extensional fracture in the Upper Amora Member. h) Extensional fault cutting slump horizons within the Lisan Formation. i) Conjugate fractures within the Upper Amora Member that converge downwards in a sandstone bed that accommodated displacement by flow.

Fig. 12 a-f) Photographs of injected clastic dykes within the Lisan Formation from near the narrower central section of the Sedom salt wall (Grid 23635550, see Fig. 3). g, i) Photographs and associated stereonets (h, j) of domino (g) and conjugate (i) extensional fractures filled by clastic dykes in the Lisan Formation. Data on stereonets h, j) is represented by: bedding (red great circles and poles by solid red squares), fractures (blue great circles and poles by solid blue circles).

Fig. 13 a-c) Photographs of conjugate gypsum veins within the Lisan Formation. Photograph d) and associated stereonet e) show gypsum-filled conjugate fractures. Data on stereonet e) is represented by: bedding (red great circles and poles by solid red squares), fractures (blue great circles and poles by solid blue circles), mean intersection of conjugate fractures (open blue circle). f) Photograph of bedding-parallel gypsum veins within the Upper Amora Member. g) Close-up of a gypsum vein from the eastern side of the Sedom salt wall with vertical fibres suggesting a 'jacking-up' of overburden..

Fig. 14 a) Photograph and associated stereonet (b) of contractional SE-dipping thrust faults within the Lisan Formation. Data on stereonet b) is represented by: bedding (red great circle and poles by solid red squares), contractional fractures (blue great circles and poles by solid blue circles). Mean poles to bedding (open red square) and fractures (open blue circle). c, d, e) Photographs of thrust planes being cut by a later clastic dyke marking extensional displacement.

Fig. 15. Schematic cross sections showing orientation and distribution of extensional fractures in drape folds next to a salt diapir. Diagrams summarise potential relationships between a) fractures that develop before drape folding, b) fractures that develop after drape folding, and c) fractures that develop during drape folding. Refer to text for further details.

Fig. 16. 3D cartoon of schematic fracture patterns and transtension along the Sedom salt wall and underlying Sedom Fault. In map view, fracture patterns define overall sigmoidal traces and rotate towards the western margin of the salt wall, while fractures fan around the northern nose of the salt wall where it plunges below the overburden. Extensional and contractional fractures are broadly synchronous and display orthogonal relationships to one another. Note that the thickness (~40 m) of the Lisan Formation is vertically exaggerated and this unit is not exposed around the eastern flank of the salt wall. Refer to text for further details.

Table 1. Mean trends of fractures in the Upper Amora Member (UAM) and overlying Lisan Formation measured towards the western margin of the Sedom salt wall. NW and SW Sedom subareas are from north and south of Grid Northing 555 respectively (see Figs. 3, 5).

Mean fracture trends tov salt contact	300 m – 200 m west of Sedom salt margin	200 m – 100 m west of Sedom salt margin	100 m –0 m west of Sed salt margin
NW Sedom Lisan Fm.	098° (N=7)	121° (N=33)	119° (N=6)
NW Sedom UAM	115° (N=35)	132° (N=43)	160° (N=33)
SW Sedom Lisan Fm.	120° (N=24)	116° (N=10)	152° (N=52)
SW Sedom UAM	140° (N=10)	154° (N=16)	152° (N=18)
Overall Lisan Fm.	109° (N=31)	118° (N=43)	144° (N=60)
Overall UAM	127° (N=45)	143° (N=59)	155° (N=51)

References

Aftabi, P., Roustaie, M**.**, Alsop, G.I.**,** Talbot, C.J. 2010. InSAR mapping and modelling of an active Iranian salt extrusion. *Journal of the Geological Society, London* 167, 155-170.

Agnon, A., Weinberger, R., Zak, I., Sneh, A. 2006. Geological Map of Israel. Sheet 20-I, II Sedom, scale 1:50,000. Israel Geological Survey, Jerusalem.

Alsop, G.I. 1996. Physical modelling of fold and fracture geometries associated with salt diapirism. In: Alsop, G.I., Blundell, D.J., Davison, I. (Eds.) Salt Tectonics. Geological Society, London, Special Publications, 100, 227-241.

Alsop, G.I., Brown J.P., Davison, I., Gibling, M.R. 2000. The geometry of drag zones adjacent to salt diapirs. *Journal of the Geological Society, London*. 157, 1019-1029.

Alsop, G.I.**,** Marco, S. 2012a. A large-scale radial pattern of seismogenic slumping towards the Dead Sea Basin. *Journal of the Geological Society* 169, 99-110.

Alsop, G.I., Marco, S. 2012b. Tsunami and seiche-triggered deformation within offshore sediments. *Sedimentary Geology* 261, 90-107.

Alsop, G.I.**,** Marco, S. 2014. Fold and fabric relationships in temporally and spatially evolving slump systems: A multi-cell flow model. *Journal of Structural Geology*, 63, 27-49.

Alsop, G.I., Weinberger, R., Levi, T., Marco, S. 2015. Deformation within an exposed salt wall: Recumbent folding and extrusion of evaporites in the Dead Sea Basin. Journal of Structural Geology, 70, 95-118.

Alsop, G.I., Weinberger, R., Levi, T., Marco, S. 2016a. Cycles of passive versus active diapirism recorded along an exposed salt wall. Journal of Structural Geology, 84, 47-67.

Alsop, G.I., Marco, S., Weinberger, R., Levi, T. 2016b. Sedimentary and structural controls on seismogenic slumping within Mass Transport Deposits from the Dead Sea Basin. Sedimentary Geology 344, 71-90.

Alsop, G.I., Marco, S., Levi, T., Weinberger, R. 2017. Fold and thrust systems in Mass Transport Deposits. Journal of Structural Geology 94, 98-115.

Al-Zoubi, A., ten Brink, U.S. 2001. Salt diapirs in the Dead Sea basin and their relationship to Quaternary extensional tectonics. Marine and Petroleum Geology, v. 18, p. 779–797.

Archer, S.G., Alsop, G.I., Hartley, A.J., Grant, N.T., Hodgkinson, R. 2012. Salt tectonics, sediments and hydrocarbon prospectivity. *In:* Alsop, G.I.**,** Archer, S.G., Hartley, A.J., Grant, N.T., Hodgkinson, R. 2012. *Salt Tectonics, Sediments and Prospectivity*. Geological Society, London, Special Publications, 363, 1-6,

Arkin, Y., Michaeli, L. 1986. The significance of shear strength in the deformation of laminated sediments in the Dead Sea area. Israel Journal of Earth Sciences 35, 61-72.

Brun, J-P., Fort, X. 2008. Entre Sel et Terre. Structures et mécanismes de la tectonique salifère. Société Géologique de France, Vuibert. pp.154. Paris, France.

Burliga, S. 2014. Heterogeneity of folding in Zechstein (Upper Permian) salt deposits in the Klowdawa salt structure, central Poland. Geological Quarterly, 58, 565-576.

Callot, J-P., Ribes, C., Kergaravat, C., Bonnel, C., Temiz, H., Poisson, A., Vrielynck, B., Salel, J-F., Ringenbach, J-C. 2014. Salt tectonics in the Sivas Basin (Turkey): crossing salt walls and minibasins. Bulletin de la de France 185, 33-42.

Carruthers, D., Cartwright, J., Jackson, M.P.A., Schutjens, P. 2013. Origin and timing of layer-bound radial faulting around North Sea salt stocks: New insights into the evolving stress state around rising diapirs. Marine and Petroleum Geology 48, 130-148.

Colon, C., Webb, A.A.G., Lasserre, C., Doin, M-P., Renard, F., Lohman, R., Li, J., Baudoin, P.F. 2016. The variety of subaerial active salt deformations in the Kuqa fold-thrust belt (China) constrained by InSAR. Earth and Planetary Science Letters 450, 83-95.

Cosgrove, J.W. 2015. The association of folds and fractures and the link between folding, fracturing and fluid flow during the evolution of a fold-thrust belt: a brief review. In: Richards, F. L., Richardson, N. J., Rippington, S. J., Wilson, R.W., Bond, C. E. (eds). Industrial Structural Geology: Principles, Techniques and Integration. Geological Society, London, Special Publications, 421, 41-68.

Davison, I., Alsop, I., Blundell, D. 1996a. Salt tectonics: some aspects of deformation mechanics. In: Alsop, G.I., Blundell, D.J., Davison, I. (Eds.) Salt Tectonics. Geological Society, London, Special Publications, 100, 1-10.

Davison, I., Bosence, D., Alsop, G.I., Al-Aawah, M.H. 1996b. Deformation and sedimentation around active Miocene salt diapirs on the Tihama Plain, northwest Yemen. In: Alsop, G.I., Blundell, D.J., Davison, I. (Eds.) Salt Tectonics. Geological Society, London, Special Publications, 100, 23-39.

Davison, I., Alsop, G.I., Evans, N.G., Safaricz, M. 2000a. Overburden deformation patterns and mechanisms of salt diapir penetration in the Central Graben, North Sea. Marine and Petroleum Geology, 17, 601-618.

Davison, I., Alsop, G.I., Birch, P., Elders, C., Evans, N., Nicholson, H., Rorison, P., Wade, D., Woodward, J., Young, M. 2000b. Geometry and late-stage structural evolution of Central Graben salt diapirs, North Sea. *Marine and Petroleum Geology* 17, 499-522.

Davison, I., Barreto, P., Andrare, A.J.M. 2017. Loulé: the anatomy of a squeezed diapir, Algarve Basin, southern Portugal. Journal of the Geological Society 174, 41-55

Dewing, K., Springer, A., Guest, B., Hadlari, T. 2016. Geological evolution and hydrocarbon potential of the salt-cored Hoodoo Dome, Sverdrup Basin, Arctic Canada. Marine and Petroleum Geology 71, 134-148.

Dooley, T.P., Jackson, M.P.A., Jackson, C, A-L., Hudec, M.R., Rodriguez, C.R. 2015a. Enigmatic structures within salt walls of the Santos Basin – Part 2: Mechanical explanation from physical modelling. Journal of Structural Geology 75, 163-187.

Dooley, T.P., Jackson, M.P.A., Hudec, M.R. 2015b. Breakout of squeezed stocks: dispersal of roof fragments, source of extrusive salt and interaction with regional thrust faults. Basin Research 27, 3-25.

Dooley, T.P., Schreurs, G. 2012. Analogue modelling of intraplate strike-slip tectonics: A review and new experimental results. Tectonophysics 574-575, 1-71.

Fossen, H. 2016. Structural Geology. 2nd edition. Cambridge University Press, Cambridge, UK. p.510.

Frumkin, A. 2009. Formation and dating of a salt pillar in Mount Sedom diapir, Israel. *Geological Society of America Bulletin*, 121, 286-293. doi:10.1130/B26376.1

Gardosh, M., Kashai, E., Salhov, S., Shulman, H., Tannenbaum, E., 1997. Hydrocarbon exploration in the southern Dead Sea area, *in* Niemi, T.M., Ben-Avraham, Z., Gat, J.R., eds., The Dead Sea: the lake and its setting: Oxford, Oxford University Press, p. 57–72.

Garfunkel, Z., 1981, Internal structure of the Dead Sea leaky transform (rift) in relation to plate kinematics: Tectonophysics, v. 80, p. 81-108.

Garfunkel, Z. 2014. Lateral motion and deformation along the Dead Sea Transform. In: Garfunkel, Z., Ben-Avraham, Z., Kagan, E. (Editors) Dead Sea Transform Fault System: Reviews. Springer Netherlands. Pages 109-150. DOI: 10.1007/978-94-017-8872-4.

Giles, K.A., Rowan, M.G. 2012. Concepts in halokinetic-sequence deformation and stratigraphy. In: Alsop, G.I., Archer, S.G., Hartley, A.J., Grant, N.T., Hodgkinson, R. (Eds.) Salt Tectonics, Sediments and Prospectivity. Geological Society, London, Special Publications, 363, 7-31.

Haase-Schramm, A., Goldstein, S.L., Stein, M. 2004. U-Th dating of Lake Lisan aragonite (late Pleistocene Dead Sea) and implications for glacial East Mediterranean climate change. Geochimica et Cosmochimica Acta 68, 985-1005.

Harding, R., Huuse, M. 2015. Salt on the move: Multi stage evolution of salt diapirs in the Netherlands North Sea. Marine and Petroleum Geology 61, 39-55.

Hearon, T.E., Rowan, M.G., Giles, K.A., Hart, W.H. 2014. Halokinetic deformation adjacent to the deepwater Auger diapir, Garden Banks, 470, northern Gulf of Mexico: Testing the applicability of an outcrop-based model using subsurface data. Interpretation 2 (4), SM57-SM76.

Hearon, T.E., Rowan, M.G., Lawton, T.F., Hannah, P.T., Giles, K.A. 2015a. Geology and tectonics of Neoproterozoic salt diapirs and salt sheets in the eastern Willouran Ranges, South Australia. Basin Research 27, 183-207.

Hearon, T.E., Rowan, M.G., Giles, K.A., Kernen, R.A., Gannaway, C.E., Lawton, T.F., Fiduk, J.C. 2015b. Allochthonous salt initiation and advance in the northern Flinders and eastern Willouran ranges, South Australia: using outcrops to test subsurface-based models from the northern Gulf of Mexico. American Association of Petroleum Geologists Bulletin 99, 293-331.

Heidari, M., Nikolinakou, M.A., Flemings, P.B., Hudec, M.R. 2017. A simplified stress analysis of rising salt domes. Basin Research 29, 363-376.

Hudec, M.R., Jackson, M.P.A. 2011. The salt mine: A digital atlas of salt tectonics. The University of Texas at Austin, Bureau of Economic Geology, Udden Book Series No. 5; American Association of Petroleum Geology Memoir 99, 305p.

Jackson, M.P.A., Hudec, M.R. 2017. Salt tectonics: Principles and practice. Cambridge University Press. UK. 510pp.

Jenyon, M. 1986. Salt tectonics. Elsevier Applied Science Publishers, London UK. pp.191

Kaproth, B.M., Kacewicz, M., Muhuri, S., Marone, C. 2016. Permeability and frictional properties of halite-clay-quartz faults in marine sediment: The role of compaction and shear. Marine and Petroleum Geology. 78, 222-235.

Karam, P., Mitra, S. 2016. Experimental studies of the controls of the geometry and evolution of salt diapirs. Marine and Petroleum Geology 77, 1309-1322.

Kaufman, A. 1971. U-series dating of Dead Sea basin carbonates: Geochimica et Cosmochimica Acta, 35, 1269–1281, doi: 10.1016/0016- 7037(71)90115-3.

Kergaravat, C., Ribes, C., Callot, J-P., Ringenbach, J-C. 2017. Tectono-stratigraphic evolution of salt-controlled minibasins in a fold and thrust belt, the Oligo-Miocene central Sivas Basin. Journal of Structural Geology 102, 75-97.

King, R., Backe, G., Tingay, M., Hillis, R., Mildren, S. 2012. Stress deflections around salt diapirs in the Gulf of Mexico. In: Healy, D., Butler, R.W.H., Shipton, Z.K., Sibson, R.H. (Editors) Faulting, fracturing and igneous intrusion in the Earth’s crust. Geological Society of London Special Publications 367, 141-153.

Koestler, A.G., Ehrmann, W.U. 1987. Fractured chalk overburden of a salt diapir, Laegerdorf, NW Germany – exposed example of a possible hydrocarbon reservoir. In: Lerche, I., O’Brien, J.J. (Editors) Dynamical geology of salt and related structures p. 457-477. Academic Press, London.

Koyi, H.A., Ghasemi, A., Hessami, K., Dietl, C. 2008. The mechanical relationship between strike-slip faults and salt diapirs in the Zagros fold-thrust belt. Journal of the Geological Society, London 165, 1031-1044.

Larsen, D.B., Ben-Avraham, Z., Shulman, H. 2002. Fault and salt tectonics in the southern Dead Sea basin. Tectonophysics 346, 71-90.

Levi, T., Weinberger, R., Aïfa, T., Eyal, Y., Marco, S., 2006. Injection mechanism of clay-rich sediments into dikes during earthquakes: Geochemistry, Geophysics, and Geosystems, v. 7, no. 12, p. Q12009

Levi, T., Weinberger, R., Eyal, Y., Lyakhovsky, V., Heifetz, E. 2008. Velocities and driving pressures of clay-rich sediments injected into clastic dykes during earthquakes. Geophysical Journal International 175, 1095-1107.

Levi, T., Weinberger, R., Eyal, Y. 2011. A coupled fluid-fracture approach to propagation of clastic dikes during earthquakes. Tectonophysics 498, 35-44.

Li, J., Webb, A.G., Mao, X., Eckhoff, I., Colon, C., Zhang, K., Wang, H., He, D. 2014. Active surface salt structures of the western Kuqa fold-thrust belt, northwestern China. Geosphere 10, 1219-1234.

Luo, G., Hudec, M.R., Flemings, P.B., Nikolinakou, M.A. 2017. Deformation, stress, and pore pressure in an evolving supra-salt basin. Journal of Geophysical Research, Solid Earth. 122, 5663-5690.

Marco, S., Weinberger, R., Agnon, A. 2002. Radial clastic dykes formed by a salt diapir in the Dead Sea Rift, Israel. Terra Nova 14, 288-294.

Martín-Martín, J.D., Vergés, J., Saura, E., Moragas, M., Messager, G., Baqués, V., Razin, P., Grélaud, C., Malaval, M., Joussiaume, R., Casciello, E., Cruz-Orosa, I., Hunt, D.W. 2017. Diaspiric growth within an Early Jurassic rift basin: The Tazoult salt wall (central High Atlas, Morocco). Tectonics 36, 2-32.

Matmon, A., Fink, D., Davis, M., Niedermann, S., Rood, D., Frumkin, A. 2014. Unravelling rift margin evolution and escarpment development ages along the Dead Sea fault using cosmogenic burial ages. Quaternary Research 82, 281-295.

Morley, C.K. 2014. Outcrop examples of soft-sediment deformation associated with normal fault terminations in deepwater, Eocene turbidites: A previously undescribed conjugate fault termination style? Journal of Structural Geology 69, 189-208.

Nikolinalou, M.A., Flemings, P.B., Hudec, M.R. 2014. Modeling stress evolution around a rising salt diapir. Marine and Petroleum Geology 51, 230-238.

Nikolinalou, M.A., Heidari, M., Hudec, M.R., Flemings, P.B., 2017. Initiation and growth of salt diapirs in tectonically stable settings: Upbuilding and megaflaps. American Association of Petroleum Geologists 101, 887-905.

Nuriel,P., Weinberger, R., Kylander-Clark, A.R.C., Hacker, B.R., Cradock, J.P. 2017. The onset of the Dead Sea transform based on calcite age-strain analyses. Geology 45, 587-590.

O'Brien, J.J., Lerch, I. 1987. Modelling of the deformation and faulting of the formations overlying an uprising salt dome. In: Lerche, I., O'Brien, J.J. (Editors) Dynamical geology of salt and related structures p. 419-455. Academic Press, London.

Palladino, G., Grippa, A., Bureau, D., Alsop, G.I., Hurst, A. 2016. Emplacement of sandstone intrusions during contractional tectonics. Journal of Structural Geology 89, 239-249.

Poprawski, Y., Basile, C., Agirrezabala, L., Jaillard, E., Gaudin, M., Jacquin, T. 2014. Sedimentary and structural record of the Albian growth of the Baikio diapir (the Basque Country, northern Spain). Basin Research, 26, 746-766.

Poprawski, Y., Basil, C., Etienne, J., Matthieu, G., Lopez, M., 2016. Halokinetic sequences in carbonate systems: An example from the Middle Albian Bakio Breccias Formation (Basque Country, Spain). Sedimentary Geology 334, 34-52.

Porat, N., Levi, T., Weinberger, R. 2007. Possible resetting of quartz OSL signals during earthquakes – evidence from late Pleistocene injection dikes, Dead Sea basin, Israel. Quaternary Geochronology 2, 272-277.

Quintà, A., Tavani, S., Roca, E. 2012. Fracture pattern analysis as a tool for constraining the interaction between regional and diapir-related stress fields: Poza de la Sal Diapir (Basque Pyrenees, Spain). In: Alsop, G.I., Archer, S.G., Hartley, A.J., Grant, N.T., Hodgkinson, R. (Eds.) Salt Tectonics, Sediments and Prospectivity. Geological Society, London, Special Publications, 363, 521-532.

Ringenbach, J-C., Salel, J-F., Kergaravat, C., Ribes, C., Bonnel, C., Callot, J-P. 2013. Salt tectonics in the Sivas Basin, Turkey: outstanding seismic analogues from outcrops. First Break 31, 93-101.

Rowan, M.G., Lawton, T.F., Giles, K.A., Ratliff, R.A. 2003. Near-diapir deformation in La Popa basin, Mexico, and the northern Gulf of Mexico: a general model for passive diapirism. American Association of Petroleum Geologists Bulletin 87, 733-756.

Rowan, M.G., Giles, K.A., Hearon, T.E., Fiduk, J.C. 2016. Megaflaps adjacent to salt diapirs. American Association of Petroleum Geologists Bulletin 100, 1723-1747.

Schofield, N., Alsop, I., Warren, J., Underhill, J.R., Lehne, R., Beer, W., Lukas, V. 2014. Mobilizing salt: Magma-salt interactions. Geology 42, 599-602.

Schorn, A., and F. Neubauer, 2014, The structure of the Hallstatt evaporite body (Northern Calcareous Alps, Austria): A compressive diapir superposed by strike-slip shear? Journal of Structural Geology, 60, 70–84.

Smit, J., Brun, J-P., Fort, X., Cloetingh, S., Ben-Avraham, Z. 2008a. Salt tectonics in pull-apart basins with application to the Dead Sea Basin. Tectonophysics, 449, 1-16.

Smit, J., Brun, J-P., Cloetingh, S., Ben-Avraham, Z. 2008b. Pull-apart basin formation and development in narrow transform zones with application to the Dead Sea Basin. Tectonics 27, TC6018

Smit, J., Brun, J-P., Cloetingh, S., Ben-Avraham, Z. 2010. The rift-like structure and asymmetry of the Dead Sea Fault. Earth and Planetary Science Letters 290, 74-82

Sneh, A., Weinberger, R. 2014. Major structures of Israel and environs, scale 1:50,000. Israel Geological Survey. Jerusalem.

Soto, R., Beamud, E., Roca, E., Carola, E., Almar, Y. 2017. Distinguishing the effect of diapir growth on magnetic fabrics of syn-diapiric overburden rocks: Basque–Cantabrian basin, Northern Spain. Terra Nova 29, 191-201.

Stewart, S. 2006. Implications of passive salt diapir kinematics for reservoir segmentation by radial and concentric faults. Marine and Petroleum Geology 23, 843-853.

Storti, F., Balsamo, F., Cappanero, F., Tosi, G. 2011. Sub-seismic scale fracture pattern and in situ permeability data in the chalk atop of the Krempe salt ridge at Lagerdorf, NW Germany: inferences on synfolding stress field evolution and its impact on fracture connectivity. Marine and Petroleum Geology 7, 1315-1332.

Talbot, C.J. 1979. Fold trains in a glacier of salt in southern Iran. Journal of Structural Geology 1, 5-18.

Talbot, C.J. 1998. Extrusions of Hormuz salt in Iran. In: Blundell, D.J., Scott, A.C. (Editors). Lyell: the Past is the Key to the Present. Geological Society, London, Special Publications 143, 315-334.

Talbot, C.J., Aftabi, P. 2004. Geology and models of salt extrusion at Qum Kuh, central Iran. Journal of the Geological Society 161, 321-334.

Torfstein, A., Haase-Schramm, A., Waldmann,N., Kolodny, Y., Stein, M. 2009. U-series and oxygen isotope chronology of the mid-Pleistocene Lake Amora (Dead Sea Basin). Geochimica et Cosmochimica Acta 73, 2603-2630.

Vargas-Meleza, L. Healy, D., Alsop, G.I., Timms, N.E. 2015. Exploring the relative contribution of mineralogy and CPO to the seismic velocity anisotropy of evaporites. Journal of Structural Geology 70, 39-55.

Vandeginste, V., Stehle, M.C., Jourdan, A.-L., Bradbury, H.J., Manning, C., Cosgrove, J.W. 2017. Diagenesis in salt dome roof strata: Barite - Calcite assemblage in Jebel Madar, Oman, Marine and Petroleum Geology 86, 408-425.

Warren, J.K. 2016. Evaporites: A geological compendium. 2nd Edition. Springer International Publishing, Switzerland. 1813pp.

Warren, J.K. 2017. Salt usually seals, but sometimes leaks: Implications for mine and cavern stability in the short and long term. Earth Science Reviews 165, 302-341.

Weinberger, R., Agnon, A., Ron, H. 1997. Paleomagnetic Reconstruction of a Diapir Emplacement: a Case Study from Sedom Diapir, the Dead Sea Rift. J. Geophys. Res.102:5173-5192.

Weinberger, R., Begin, Z.B., Waldmann, N., Gardosh, M., Baer, G., Frumkin, A., Wdowinski, S. 2006a. Quaternary rise of the Sedom diapir, Dead Sea basin. In: New Frontiers in Dead Sea Paleoenvironmental Research, (Enzel, Y. Agnon, A., Stein, M., eds). Geol. Soc. Am. Special Paper, 401, 33-51

Weinberger, R., Lyakhovsky, V., Baer, G., and Begin, Z. B. 2006b. Mechanical modeling and InSAR measurements of Mount Sedom uplift, Dead Sea Basin: Implications for rock-salt properties and diapir emplacement mechanism. Geochem. Geophys. Geosyst. 7, Q05014

Weinberger, R., Bar-Matthews, M., Levi, T., Begin, Z.B. 2007. Late-Pleistocene rise of the Sedom diapir on the backdrop of water-level fluctuations of Lake Lisan, Dead Sea basin. Quaternary International 175, 53-61

Weinberger, R., Levi, T., Alsop. G.I., Eyal, Y. 2016. Coseismic horizontal slip revealed by sheared clastic dikes in the Dead Sea basin. Geological Society of America Bulletin 128, 1193-1206.

Wu, L., Trudgill, B.D., Kluth, C.F. 2016. Salt diapir reactivation and normal faulting in an oblique extensional system, Vulcan sub-basin, NW Australia. Journal of the Geological Society 173, 783-799.

Yin, H., Groshong, R.H. 2007. A three-dimensional kinematic model for the deformation above an active diapir. American Association of Petroleum Geologists 91, 343-363.

Zak, I., 1967. The geology of Mount Sedom [Ph.D. thesis]: The Hebrew University of Jerusalem, 208 p. (in Hebrew with an English abstract).

Zak, I., Freund, R. 1980. Strain measurements in eastern marginal shear zone of Mount Sedom salt diapir, Israel: AAPG Bulletin, v. 64, p. 568–581.

Zak, I., Karcz, I., Key, C.A. 1968. Significance of some sedimentary structures from Mount Sedom: Israel Journal of Earth Sciences, v. 17, p. 1–8.

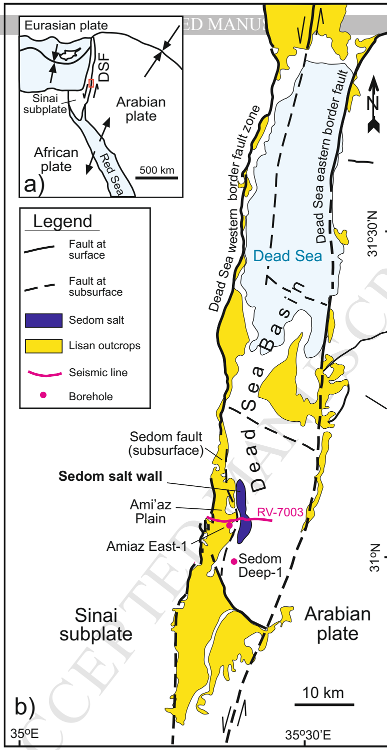
Eurasian plate
DSF
Sinai
subplate
Arabian
plate
African
plate
Red Sea
500 km
a)
Legend
Fault at
surface
Fault at
subsurface
Sedom salt
Lisan outcrops
Seismic line
Borehole
Dead Sea western border fault zone
Dead Sea eastern border fault
N
31°30'N
Dead Sea
Dead Sea Basin
Sedom fault
(subsurface)
Sedom salt wall
Ami'az
Plain
RV-7003
Amiaz East-1
Sedom
Deep-1
31°N
Sinai
subplate
Arabian
plate
10 km
b)
35°E
35°30'E

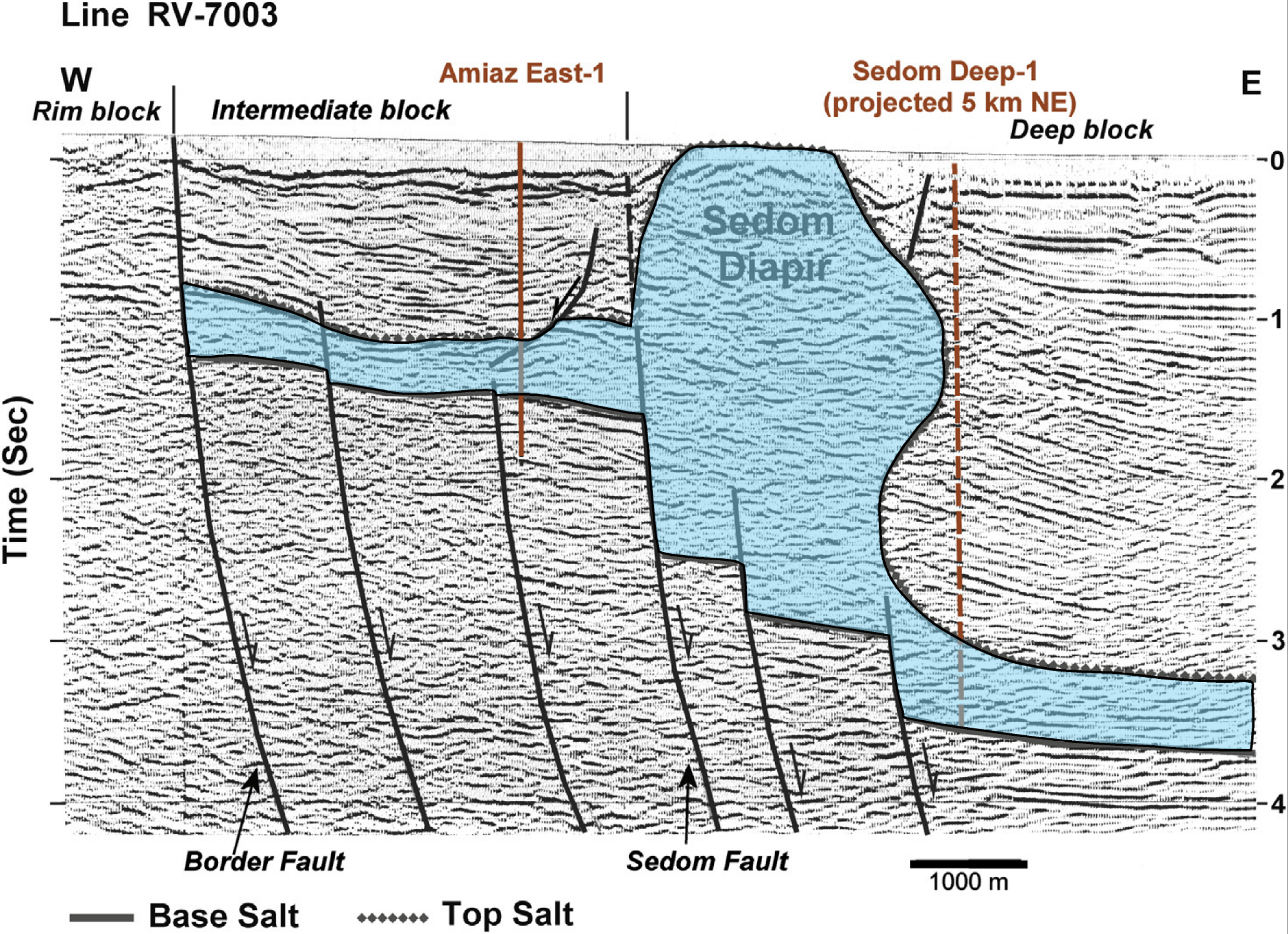
Line RV-7003
W
Rim block
Intermediate block
Amiaz East-1
Sedom Deep-1
(projected 5 km NE)
E
Deep block
Sedom
Diapir
Time (Sec)
0
1
2
3
4
Border Fault
Sedom Fault
1000 m
Base Salt
Top Salt

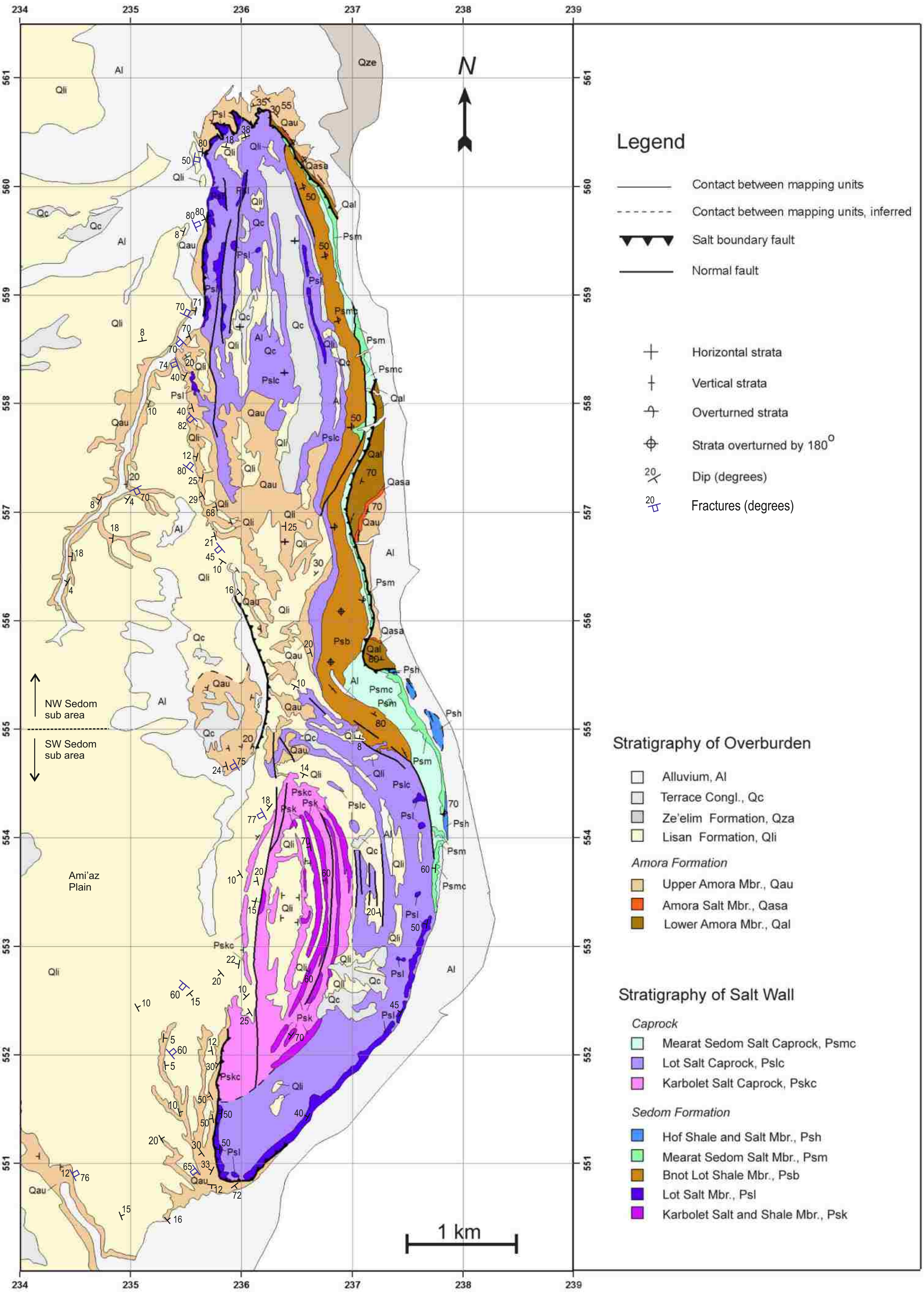

N
Legend
Contact between mapping units
Contact between mapping units, inferred
Salt boundary fault
Normal fault
Horizontal strata
Vertical strata
Overturned strata
Strata overturned by 180°
Dip (degrees)
Fractures (degrees)
Stratigraphy of Overburden
Alluvium, Al
Terrace Congl., Qc
Ze'elim Formation, Qza
Lisan Formation, Qli
Amora Formation
Upper Amora Mbr., Qau
Amora Salt Mbr., Qasa
Lower Amora Mbr., Qal
Stratigraphy of Salt Wall
Caprock
Mearat Sedom Salt Caprock, Psmc
Lot Salt Caprock, Pslc
Karbolet Salt Caprock, Pskc
Sedom Formation
Hof Shale and Salt Mbr., Psh
Mearat Sedom Salt Mbr., Psm
Bnot Lot Shale Mbr., Psb
Lot Salt Mbr., Psl
Karbolet Salt and Shale Mbr., Psk
NW Sedom sub area
SW Sedom sub area
Ami'az Plain
1 km
234
235
236
237
238
239
561
560
559
558
557
556
555
554
553
552
551

Formation	Member	Description and Age
Lisan Formation		40 m of aragonite-rich lacustrine sediments dated between ~70 ka and 14 ka (U-series and ^{14}C, Kaufman, 1971; Haase-Schramm et al., 2004).
Amora Formation (overburden to Sedom salt wall)	**Upper Amora Member**	200 m of fluvio-lacustrine shales, sandstones and conglomerates ranging in age between 340 – 80 ka (Torfstein et al., 2009).
	Amora Salt Member	10 m thick halite unit dated at 420 ± 10 ka (U-Th ages from Torfstein et al., 2009)
	Lower Amora Member	200 m of fluvio-lacustrine shales, sandstones and conglomerates exposed at outcrop. Dated at 740 ± 66 ka (U series ages from Torfstein et al., 2009). The base of the Amora Formation in the Ami'az 1 borehole is dated at 3.3 ± 0.9 Ma (^{10}Be TCN burial ages from Matmon et al., 2014).
Sedom Formation (forms the Sedom salt wall)	**Hof Shale and Salt Member**	Up to 90 m of halite and shales (Zak et al., 1968)
	Mearat Sedom Salt Member	Up to 250 m of halite, anhydrite and minor clastics
	Bnot Lot Shales Member	Up to 200 m thick sandstones and shales dated at 6.2 and 5.0 ± 0.5 Ma (^{10}Be TCN burial ages from Matmon et al., 2014)
	Lot Salt Member	Up to 800 m of halite, anhydrite and minor clastics
	Karbolet Salt and Shale Member	550 m minimum thickness of halite and shale units (base not observed and not dated).

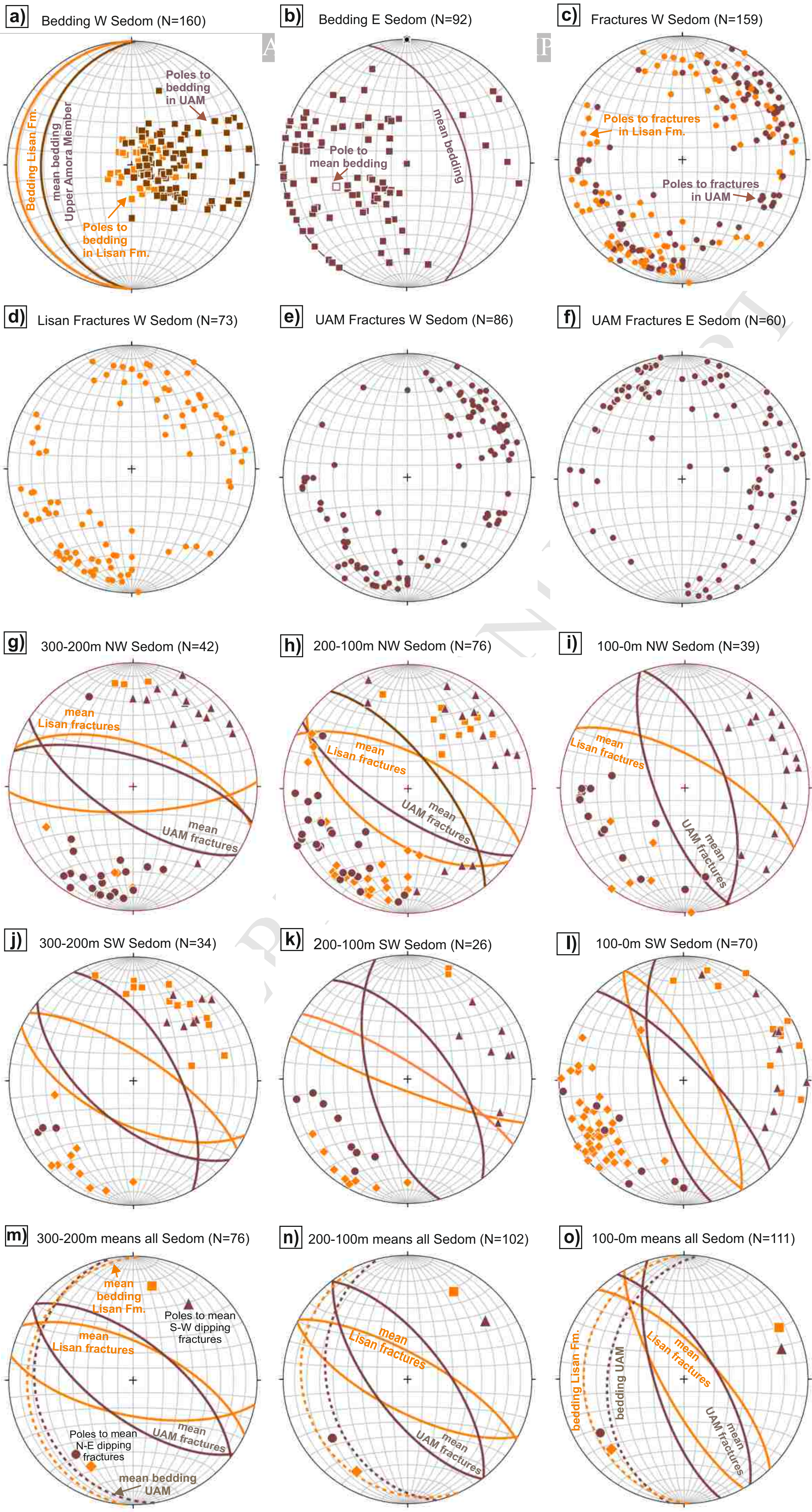

a) Bedding W Sedom (N=160)
Poles to bedding in UAM
Bedding Lisan Fm.
mean bedding Upper Amora Member
Poles to bedding in Lisan Fm.
b) Bedding E Sedom (N=92)
mean bedding
Pole to mean bedding
c) Fractures W Sedom (N=159)
Poles to fractures in Lisan Fm.
Poles to fractures in UAM
d) Lisan Fractures W Sedom (N=73)
e) UAM Fractures W Sedom (N=86)
f) UAM Fractures E Sedom (N=60)
g) 300-200m NW Sedom (N=42)
mean Lisan fractures
mean UAM fractures
h) 200-100m NW Sedom (N=76)
mean Lisan fractures
mean UAM fractures
i) 100-0m NW Sedom (N=39)
mean Lisan fractures
mean UAM fractures
j) 300-200m SW Sedom (N=34)
k) 200-100m SW Sedom (N=26)
l) 100-0m SW Sedom (N=70)
m) 300-200m means all Sedom (N=76)
mean bedding Lisan Fm.
Poles to mean S-W dipping fractures
mean Lisan fractures
mean UAM fractures
Poles to mean N-E dipping fractures
mean bedding UAM
n) 200-100m means all Sedom (N=102)
mean Lisan fractures
mean UAM fractures
o) 100-0m means all Sedom (N=111)
bedding Lisan Fm.
bedding UAM
mean Lisan fractures
mean UAM fractures

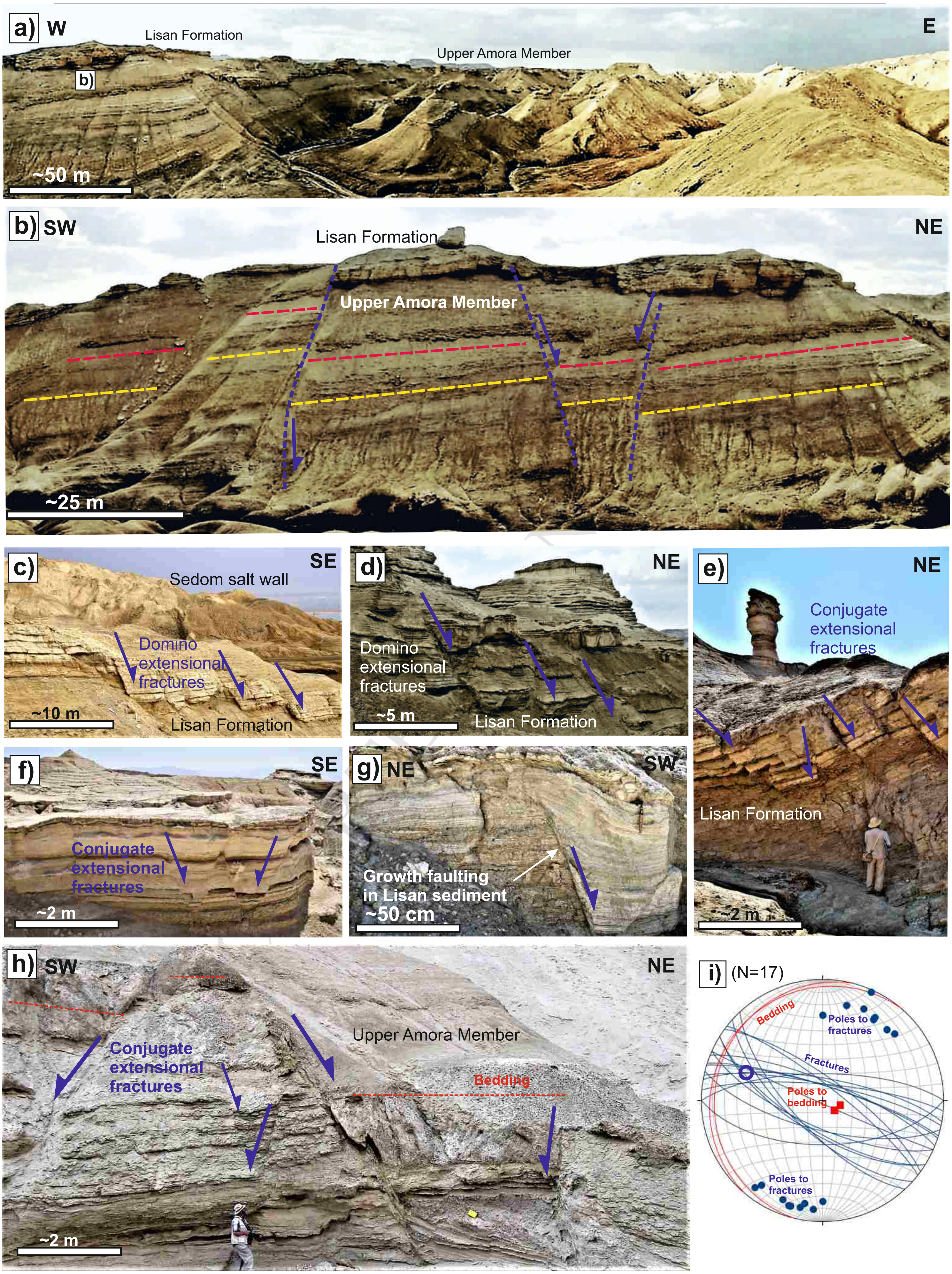

a) W
E
Lisan Formation
Upper Amora Member
b)
~50 m
b) SW
NE
Lisan Formation
Upper Amora Member
~25 m
c)
SE
Sedom salt wall
Domino extensional fractures
~10 m
Lisan Formation
d)
NE
Domino extensional fractures
~5 m
Lisan Formation
e)
NE
Conjugate extensional fractures
Lisan Formation
~2 m
f)
SE
Conjugate extensional fractures
~2 m
g) NE
SW
Growth faulting in Lisan sediment
~50 cm
h) SW
NE
Conjugate extensional fractures
Upper Amora Member
Bedding
~2 m
i) (N=17)
Bedding
Poles to fractures
Fractures
Poles to bedding
Poles to fractures

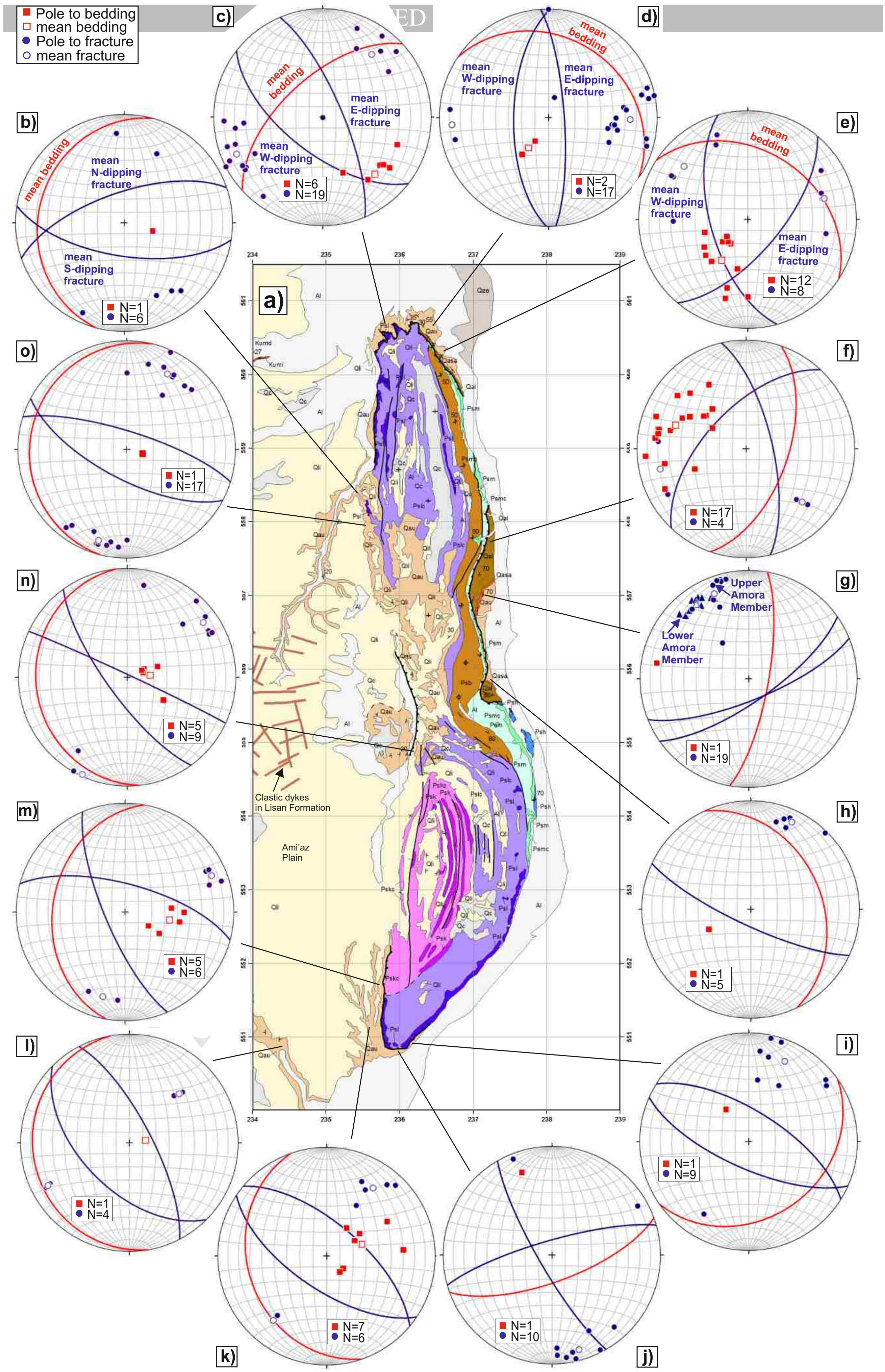
Pole to bedding
mean bedding
Pole to fracture
mean fracture
a)
b)
mean bedding
mean N-dipping fracture
mean S-dipping fracture
N=1
N=6
c)
mean bedding
mean E-dipping fracture
mean W-dipping fracture
N=6
N=19
d)
mean bedding
mean W-dipping fracture
mean E-dipping fracture
N=2
N=17
e)
mean bedding
mean W-dipping fracture
mean E-dipping fracture
N=12
N=8
f)
N=17
N=4
g)
Upper Amora Member
Lower Amora Member
N=1
N=19
h)
N=1
N=5
i)
N=1
N=9
j)
N=1
N=10
k)
N=7
N=6
l)
N=1
N=4
m)
N=5
N=6
n)
N=5
N=9
o)
N=1
N=17
Clastic dykes in Lisan Formation
Ami'az Plain
234
235
236
237
238
239

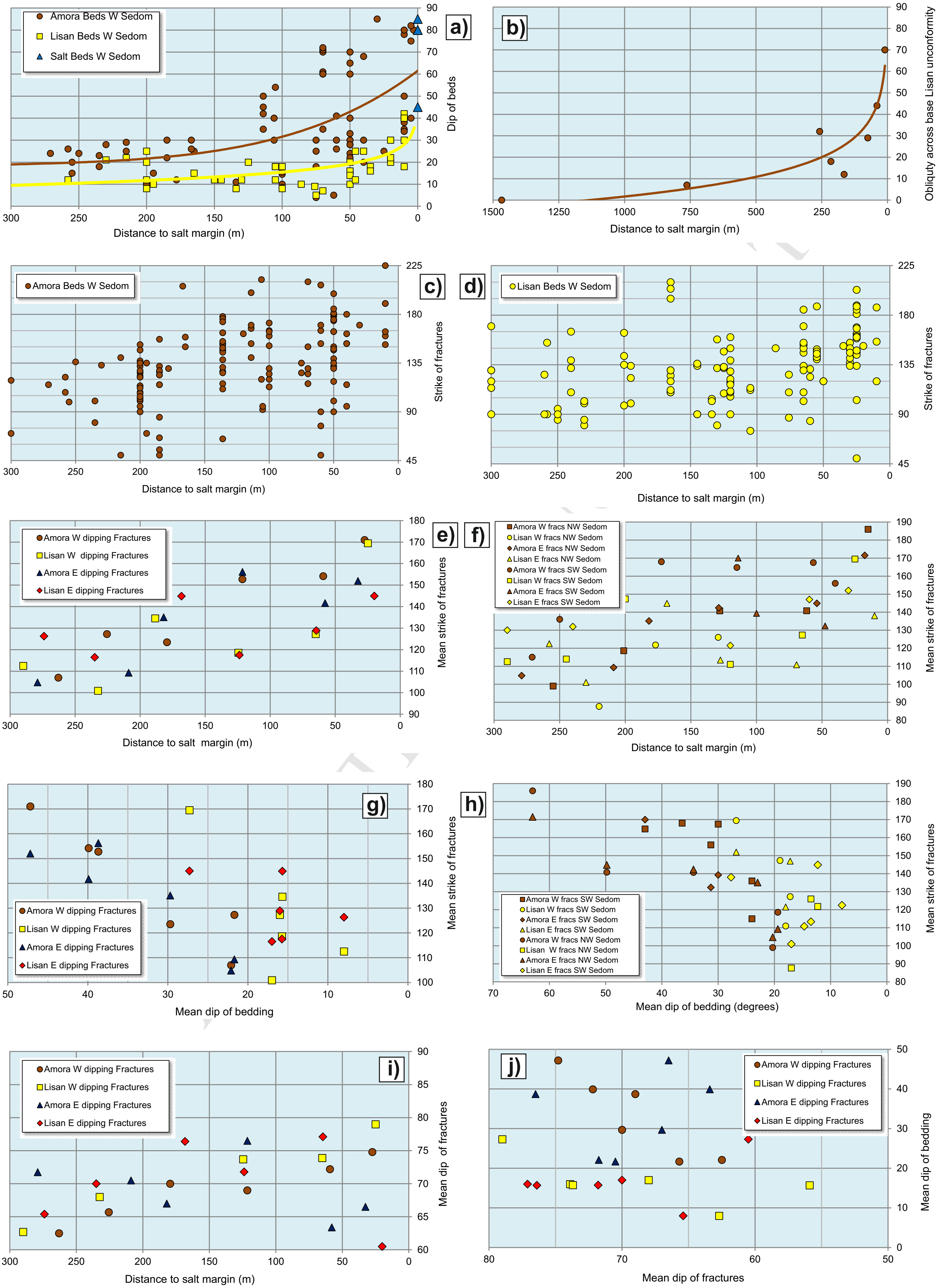
a)
Amora Beds W Sedom
Lisan Beds W Sedom
Salt Beds W Sedom
Dip of beds
Distance to salt margin (m)
b)
Obliquity across base Lisan unconformity
Distance to salt margin (m)
c)
Amora Beds W Sedom
Strike of fractures
Distance to salt margin (m)
d)
Lisan Beds W Sedom
Strike of fractures
Distance to salt margin (m)
e)
Amora W dipping Fractures
Lisan W dipping Fractures
Amora E dipping Fractures
Lisan E dipping Fractures
Mean strike of fractures
Distance to salt margin (m)
f)
Amora W fracs NW Sedom
Lisan W fracs NW Sedom
Amora E fracs NW Sedom
Lisan E fracs NW Sedom
Amora W fracs SW Sedom
Lisan W fracs SW Sedom
Amora E fracs SW Sedom
Lisan E fracs SW Sedom
Mean strike of fractures
Distance to salt margin (m)
g)
Amora W dipping Fractures
Lisan W dipping Fractures
Amora E dipping Fractures
Lisan E dipping Fractures
Mean dip of bedding
h)
Amora W fracs SW Sedom
Lisan W fracs SW Sedom
Amora E fracs SW Sedom
Lisan E fracs SW Sedom
Amora W fracs NW Sedom
Lisan W fracs NW Sedom
Amora E fracs NW Sedom
Lisan E fracs SW Sedom
Mean strike of fractures
Mean dip of bedding (degrees)
i)
Amora W dipping Fractures
Lisan W dipping Fractures
Amora E dipping Fractures
Lisan E dipping Fractures
Mean dip of fractures
Distance to salt margin (m)
j)
Amora W dipping Fractures
Lisan W dipping Fractures
Amora E dipping Fractures
Lisan E dipping Fractures
Mean dip of bedding
Mean dip of fractures

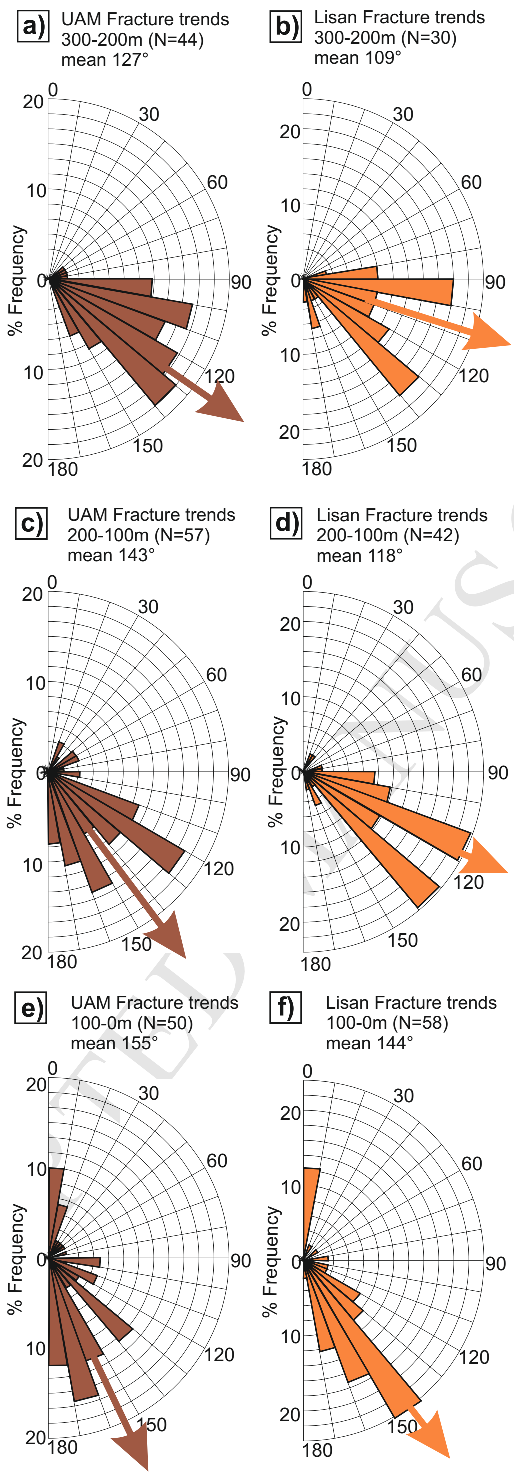
a)
UAM Fracture trends
300-200m (N=44)
mean 127°
b)
Lisan Fracture trends
300-200m (N=30)
mean 109°
c)
UAM Fracture trends
200-100m (N=57)
mean 143°
d)
Lisan Fracture trends
200-100m (N=42)
mean 118°
e)
UAM Fracture trends
100-0m (N=50)
mean 155°
f)
Lisan Fracture trends
100-0m (N=58)
mean 144°
% Frequency
0
30
60
90
120
150
180
10
20

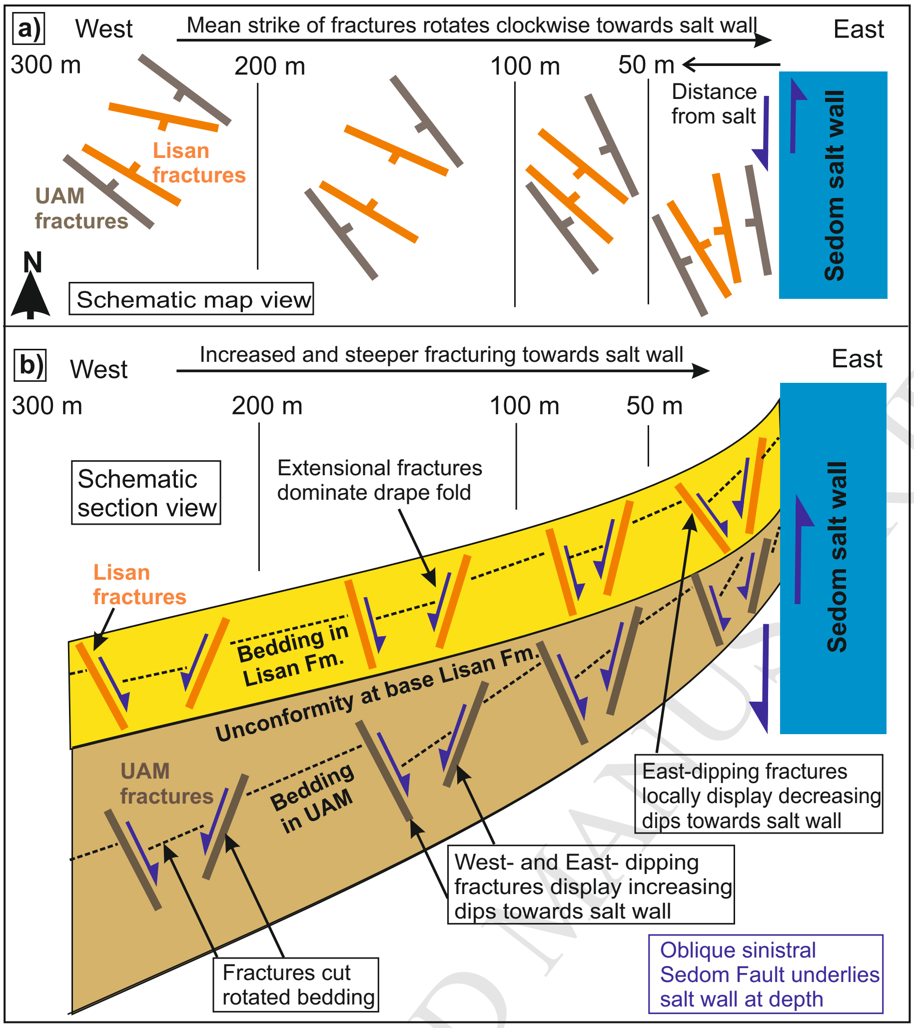

a)
West
Mean strike of fractures rotates clockwise towards salt wall
East
300 m
200 m
100 m
50 m
Distance from salt
Lisan fractures
UAM fractures
N
Schematic map view
Sedom salt wall
b)
West
Increased and steeper fracturing towards salt wall
East
300 m
200 m
100 m
50 m
Schematic section view
Extensional fractures dominate drape fold
Lisan fractures
Bedding in Lisan Fm.
Unconformity at base Lisan Fm.
UAM fractures
Bedding in UAM
Sedom salt wall
East-dipping fractures locally display decreasing dips towards salt wall
West- and East- dipping fractures display increasing dips towards salt wall
Fractures cut rotated bedding
Oblique sinistral Sedom Fault underlies salt wall at depth

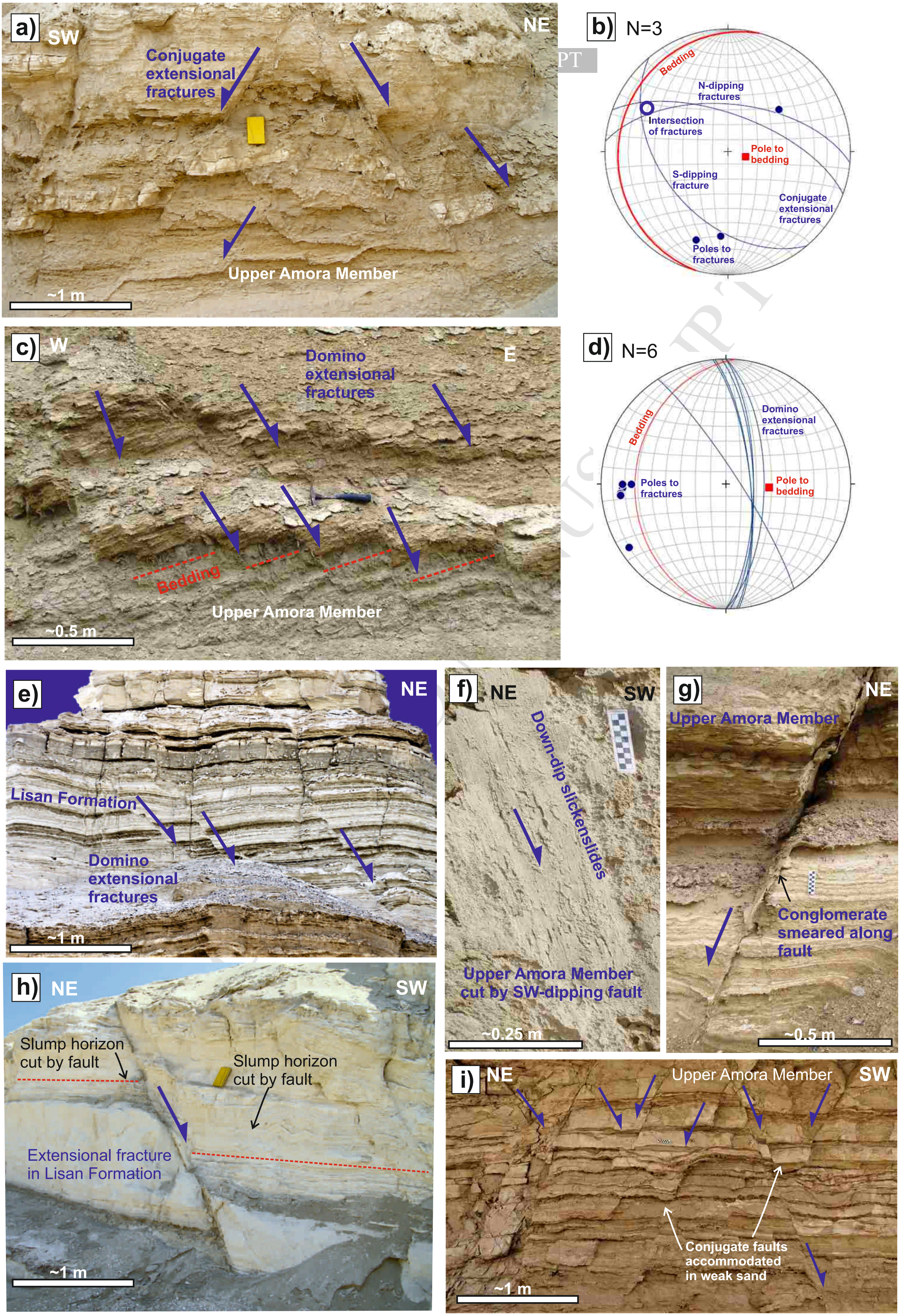

a)
SW
NE
Conjugate extensional fractures
Upper Amora Member
~1 m
b)
N=3
Bedding
N-dipping fractures
Intersection of fractures
Pole to bedding
S-dipping fracture
Conjugate extensional fractures
Poles to fractures
c)
W
E
Domino extensional fractures
Bedding
Upper Amora Member
~0.5 m
d)
N=6
Domino extensional fractures
Bedding
Poles to fractures
Pole to bedding
e)
NE
Lisan Formation
Domino extensional fractures
~1 m
f)
NE
SW
Down-dip slickenslides
Upper Amora Member cut by SW-dipping fault
~0.25 m
g)
NE
Upper Amora Member
Conglomerate smeared along fault
~0.5 m
h)
NE
SW
Slump horizon cut by fault
Slump horizon cut by fault
Extensional fracture in Lisan Formation
~1 m
i)
NE
Upper Amora Member
SW
Conjugate faults accommodated in weak sand
~1 m

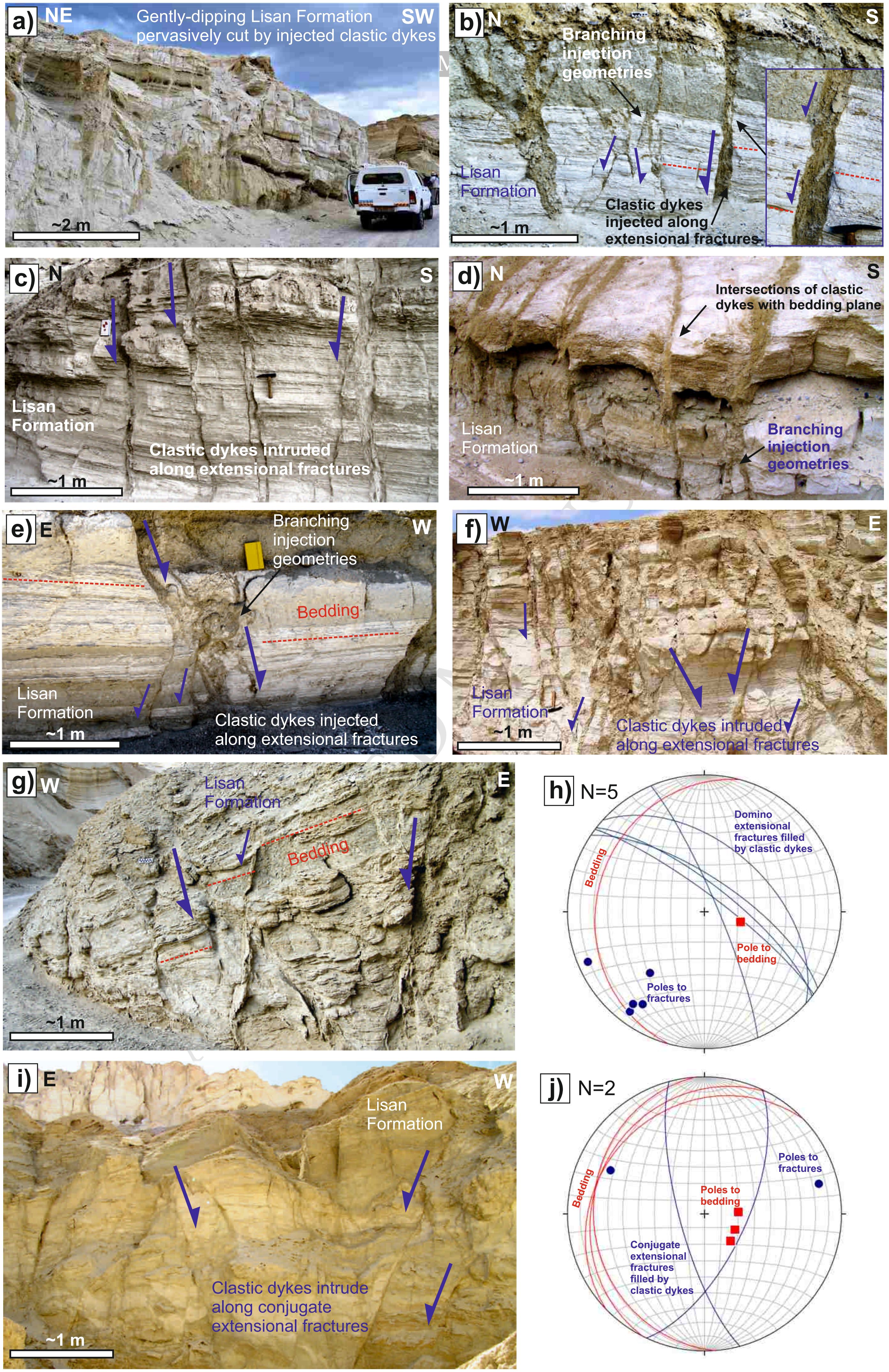
a) NE
Gently-dipping Lisan Formation pervasively cut by injected clastic dykes
SW
~2 m
b) N
S
Branching injection geometries
Lisan Formation
Clastic dykes injected along extensional fractures
~1 m
c) N
S
Lisan Formation
Clastic dykes intruded along extensional fractures
~1 m
d) N
S
Intersections of clastic dykes with bedding plane
Lisan Formation
Branching injection geometries
~1 m
e) E
W
Branching injection geometries
Bedding
Lisan Formation
Clastic dykes injected along extensional fractures
~1 m
f) W
E
Lisan Formation
Clastic dykes intruded along extensional fractures
~1 m
g) W
E
Lisan Formation
Bedding
~1 m
h) N=5
Domino extensional fractures filled by clastic dykes
Bedding
Pole to bedding
Poles to fractures
i) E
W
Lisan Formation
Clastic dykes intrude along conjugate extensional fractures
~1 m
j) N=2
Poles to fractures
Bedding
Poles to bedding
Conjugate extensional fractures filled by clastic dykes

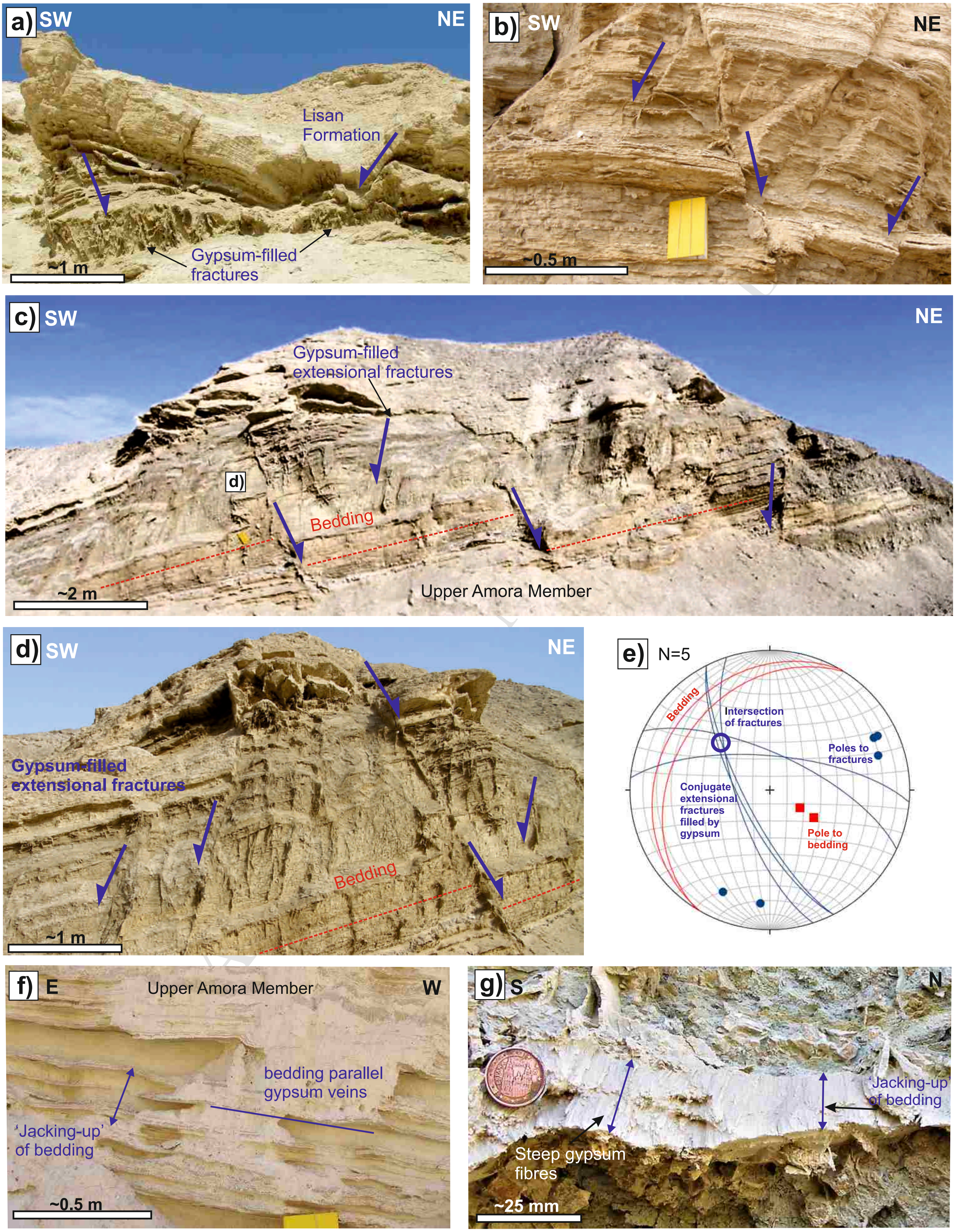
a) SW
NE
Lisan
Formation
Gypsum-filled
fractures
~1 m
b) SW
NE
~0.5 m
c) SW
NE
Gypsum-filled
extensional fractures
d)
Bedding
Upper Amora Member
~2 m
d) SW
NE
Gypsum-filled
extensional fractures
Bedding
~1 m
e) N=5
Bedding
Intersection
of fractures
Poles to
fractures
Conjugate
extensional
fractures
filled by
gypsum
Pole to
bedding
f) E
Upper Amora Member
W
bedding parallel
gypsum veins
'Jacking-up'
of bedding
~0.5 m
g) S
N
'Jacking-up'
of bedding
Steep gypsum
fibres
~25 mm

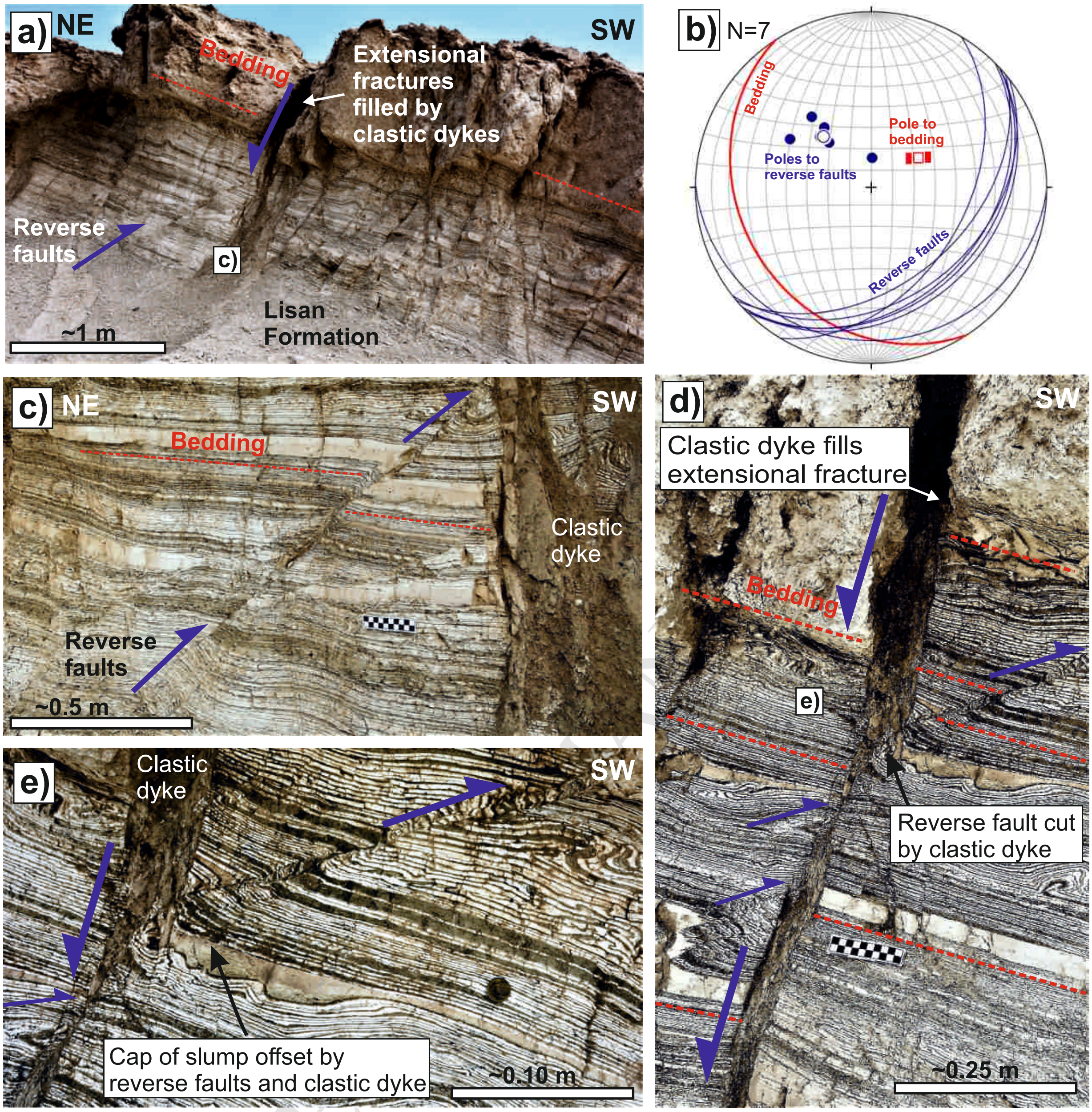

a)
NE
SW
Bedding
Extensional fractures filled by clastic dykes
Reverse faults
c)
~1 m
Lisan Formation
b)
N=7
Bedding
Pole to bedding
Poles to reverse faults
Reverse faults
c)
NE
SW
Bedding
Clastic dyke
Reverse faults
~0.5 m
d)
SW
Clastic dyke fills extensional fracture
Bedding
e)
Reverse fault cut by clastic dyke
~0.25 m
e)
Clastic dyke
SW
Cap of slump offset by reverse faults and clastic dyke
~0.10 m

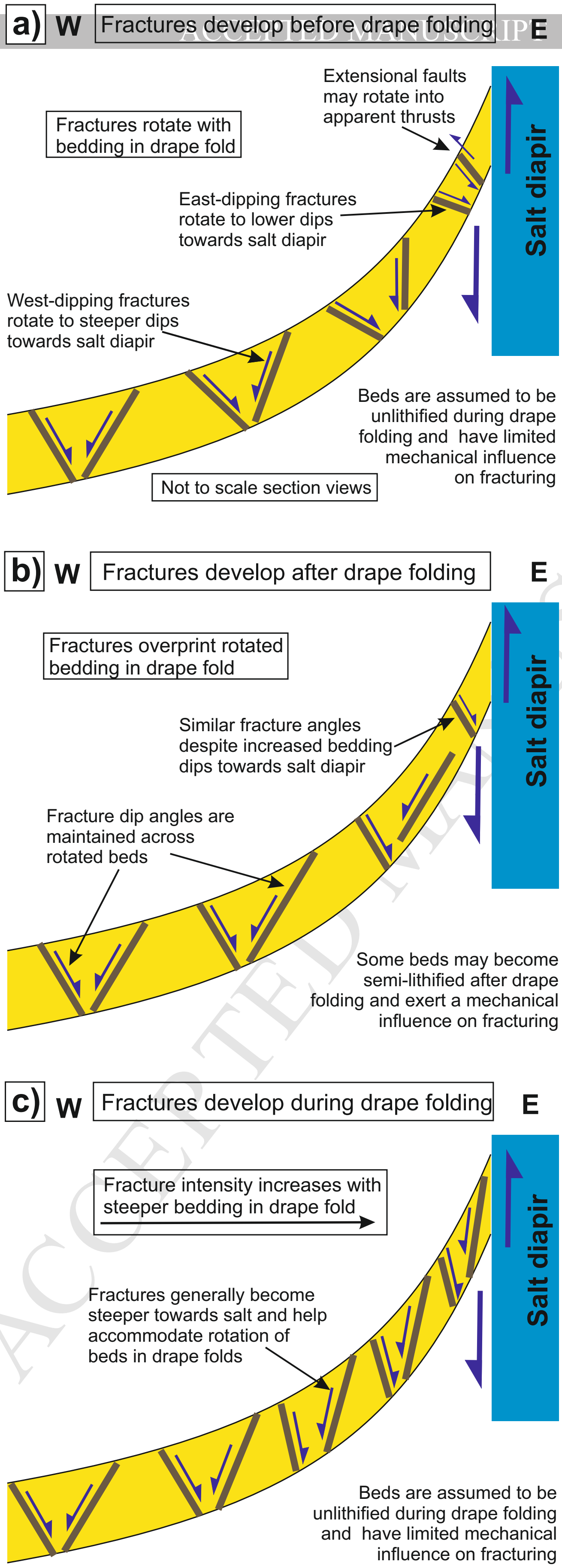

a) W
Fractures develop before drape folding
E
Extensional faults may rotate into apparent thrusts
Fractures rotate with bedding in drape fold
Salt diapir
East-dipping fractures rotate to lower dips towards salt diapir
West-dipping fractures rotate to steeper dips towards salt diapir
Beds are assumed to be unlithified during drape folding and have limited mechanical influence on fracturing
Not to scale section views
b) W
Fractures develop after drape folding
E
Fractures overprint rotated bedding in drape fold
Salt diapir
Similar fracture angles despite increased bedding dips towards salt diapir
Fracture dip angles are maintained across rotated beds
Some beds may become semi-lithified after drape folding and exert a mechanical influence on fracturing
c) W
Fractures develop during drape folding
E
Fracture intensity increases with steeper bedding in drape fold
Salt diapir
Fractures generally become steeper towards salt and help accommodate rotation of beds in drape folds
Beds are assumed to be unlithified during drape folding and have limited mechanical influence on fracturing

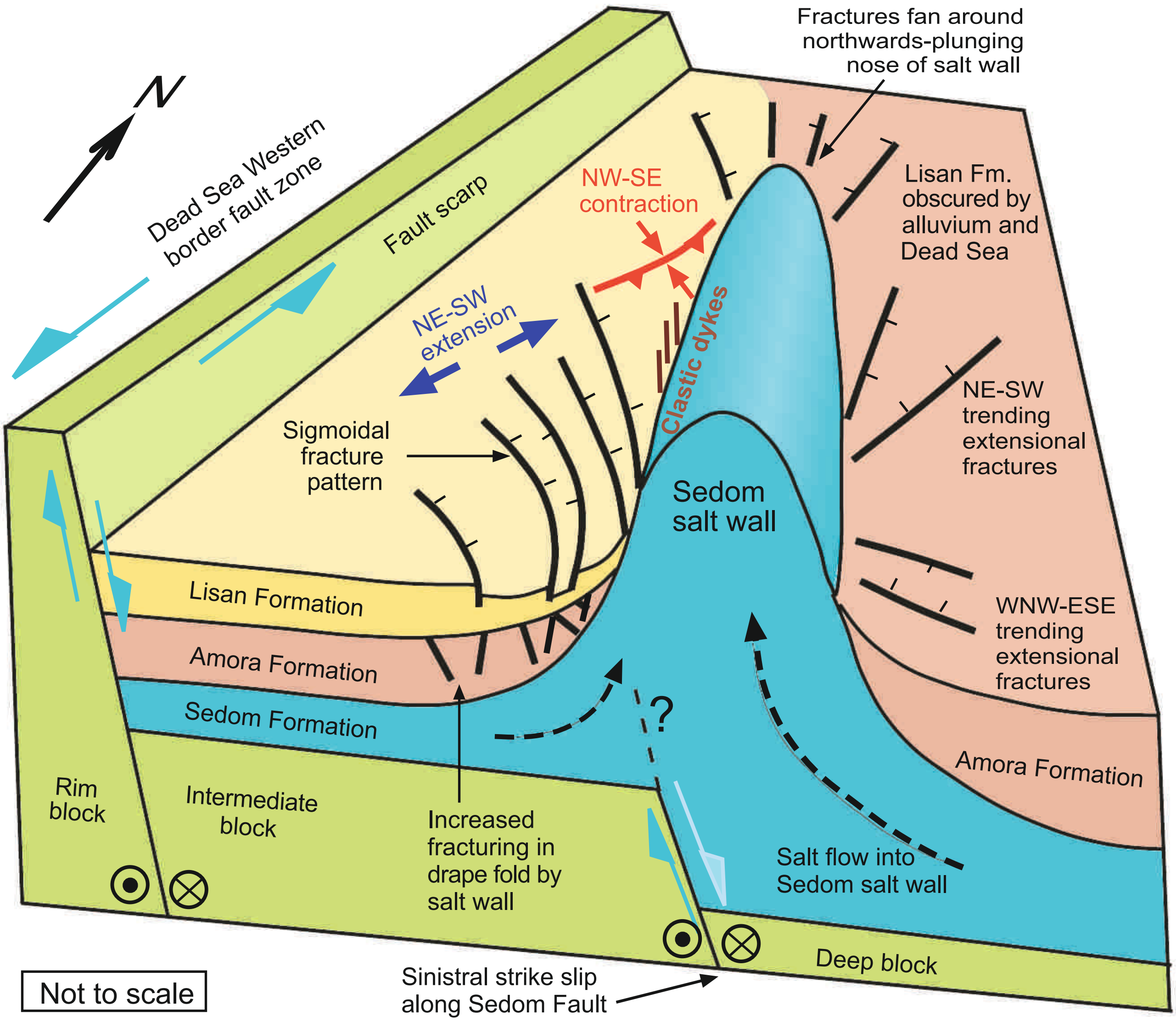

Fractures fan around northwards-plunging nose of salt wall
N
Dead Sea Western border fault zone
Fault scarp
NW-SE contraction
Lisan Fm. obscured by alluvium and Dead Sea
NE-SW extension
Clastic dykes
NE-SW trending extensional fractures
Sigmoidal fracture pattern
Sedom salt wall
Lisan Formation
WNW-ESE trending extensional fractures
Amora Formation
?
Sedom Formation
Amora Formation
Rim block
Intermediate block
Increased fracturing in drape fold by salt wall
Salt flow into Sedom salt wall
Deep block
Not to scale
Sinistral strike slip along Sedom Fault

Fault and fracture patterns are examined around an exposed salt wall in the Dead Sea Basin.

Drape folding is marked by extensional fractures that help accommodate upturn of overburden.

Fracture patterns are neither concentric nor radial where diapirism is influenced by regional tectonics.

Regional strike-slip faulting results in sigmoidal fracture traces developed at 45° to the salt wall.

Injected clastic dykes and gypsum veins develop due to high fluid pressures adjacent to the salt wall.